

Radiation Data Reduction Procedures for Sabreliner, C-130, and DC-6 Aircraft During the Garp Atlantic Tropical Experiment

By
Bruce A. Albrecht and Stephen K. Cox

Department of Atmospheric Science
Colorado State University
Fort Collins, Colorado

The activities reported in this paper have been supported by the Global Atmospheric Research Program, National Science Foundation and the GATE Project Office, NOAA, under Grants OCD72-01681 and COD74-21678.

February 1976



**Department of
Atmospheric Science**

Paper No. 244

RADIATION DATA REDUCTION PROCEDURES
FOR SABRELINER, C-130, and DC-6 AIRCRAFT
DURING THE GARP ATLANTIC TROPICAL EXPERIMENT

by
Bruce A. Albrecht
and
Stephen K. Cox

The activities reported in this paper have been supported by
the Global Atmospheric Research Program, National Science
Foundation and the GATE Project Office, NOAA, under Grants
OCD 72-01681 A04 and COD 74 21678.

Department of Atmospheric Science
Colorado State University
Fort Collins, Colorado
80523

February 1976

Atmospheric Science Paper Number 244

PREFACE

A primary objective of the GATE field phases was to make available a basic data set describing the characteristics of the disturbed and undisturbed tropical atmosphere. While the collection of the data is an essential step toward this goal, it is equally essential to make detailed information available on instrument characteristics, instrument performance, reduction procedures, etc., so that scientific users may become knowledgeable about the dependability and quality of the data.

It is the purpose of this report to collect and present this information for the U.S. C-130, DC-6 and Sabreliner broadband shortwave and longwave irradiance data to become available during Spring 1976. With the information presented in this report, a scrupulous user of these data will be able to trace the entire history of the data and make quality judgements of his own.

Hopefully, this report will make the basic aircraft radiation data easier to use and will result in a better qualified and broader user audience.

TABLE OF CONTENTS

	<u>PAGE</u>
PREFACE	
ABSTRACT	1
1.0 INTRODUCTION	2
2.0 DESCRIPTION OF RADIATION MEASUREMENT SYSTEMS	3
2.1 U.S. C-130 and DC-6 Systems	3
2.2 Sabreliner System	8
3.0 THEORY OF OPERATION OF BROADBAND HEMISPHERIC RADIATION SENSORS	9
3.1 Precision Pyranometer (SW)	9
3.2 Precision Infrared Radiometers (LW)	9
3.21 Precision Infrared Radiometer Laboratory Calibration Procedure	10
4.0 CALIBRATION AND DATA REDUCTION	15
4.1 Sensors	15
4.2 Amplifier/Data System Calibrations	15
4.3 First Order Data Reduction Equation Factors	15
4.4 Higher Order Corrections Applied to Data Reduction	20
4.5 Corrections to SW Data	20
4.51 Geometry Correction for Non-Horizontal Sensor	20
4.52 Temperature Correction	21
4.521 Sabreliner	21
4.522 NOAA C-130	21
4.523 NOAA DC-6	21
4.6 Corrections to the LW Data	26
4.61 Sabreliner	26
4.62 NOAA C-130 Self Emission Correction	31
4.63 NOAA DC-6	38
4.631 Self Emission Correction	38
4.632 Solar Heating of DC-6 Pyrgeometer KRS-5 Dome	38
5.0 CONCLUDING REMARKS	39
ACKNOWLEDGEMENTS	41

TABLE OF CONTENTS - Continued

	<u>PAGE</u>
APPENDIX A. Temperature Corrected Aircraft Pyrgeometer Measurements	42
A.I Introduction	45
A.II Pyrgeometer Performance: Theoretical vs. Actual	46
A.III Pyrgeometer Corrections	49
A. Battery Voltage Uncertainties	49
B. Non-Linearity of Pyrgeometer Temperature Compensation Circuitry	51
C. Dome-Sink Temperature Differences	53
A.IV Application of Corrections to Real Data	58
A.V Conclusions and Recommendations	67
APPENDIX B. DC-6 Solar Heating Correction for LW \downarrow Measurements	70
B.I Introduction	72
B.II Method of Correction	72
B.III Results	80
B.IV Conclusions	83
APPENDIX C. Data Flagging Criteria	84
APPENDIX D. GATE DC-6 "Quick-Look" Comments	90
APPENDIX E. GATE Sabreliner "Quick-Look" Comments	93
APPENDIX F. GATE C-130 "Quick-Look" Comments	96
APPENDIX G. Magnetic Tape Data Formats for Aircraft Reduced Data	99

LIST OF TABLES

<u>TABLE</u>		<u>PAGE</u>
I	Calibration factors for U.S. C-130.	17
II	Calibration factors for U.S. DC-6.	18
III	Calibration factors for NCAR Sabreliner.	19
IV	K_3 as a function of temperature.	22
V	K_4 as a function of temperature.	23
VI	K_5 as a function of temperature.	24
VII	K_6 as a function of temperature.	25
VIII	K_7 as a function of temperature.	27
IX	K_8 as a function of temperature.	28
X	Sabreliner battery voltage as a function of Julian Day.	29
XI	Sabreliner L_B/E_0 as a function of instrument temperature.	30
XIIa	K_1 as a function of temperature - Julian Days 197-240 only.	32
XIIb	K_1 as a function of temperature - Julian Days 241-262 only.	33
XIIIa	K_2 as a function of temperature - Julian Days 197-240 only.	34
XIIIb	K_2 as a function of temperature - Julian Days 241-262 only.	35
XIV	Four additional channels on the Sabreliner used to record the temperature of the dome and sink of the LW sensors.	36
XV	δL as a function of temperature.	37
XVI	Listing of aircraft broadband radiation data problems noted to date.	40
APPENDIX C		
C1	Meaning of flag numbers.	85
C2	Criteria used to assign a numerical flag value for C-130 and DC-6 radiation data.	86

LIST OF TABLES - Continued

<u>TABLE</u>		<u>PAGE</u>
C3	Data quality flagging criteria for Sabreliner radiation data	87
C4	Analytical approximations to the $H_{\max}(t)$ values given in Table C1	88
C5	Maximum possible rate of change of GATE aircraft radiation parameters.	89

LIST OF FIGURES

<u>FIGURE</u>		<u>PAGE</u>
1	Basic radiation measurement system.	4
2	Photograph of inside of pod.	5
3	Photograph of pod mounted on DC-6 aircraft.	6
4	Photograph of pod mounted on C-130 aircraft.	7
5	Variation of dome and sink pyrgeometer temperatures as a function of time during a blackbody calibration.	11
6	Thermopile output as a function of the difference in the radiative energy per unit area emitted by the blackbody and the thermopile surface.	13
7	$L - \epsilon_S \sigma T_S^4 - E/\eta$ as a function of $(\sigma T_d^4 - \sigma T_S^4)$. The coefficient k is given by the slope of these points. T_{BB} is the approx. blackbody temperature at each calibration point.	14
 APPENDIX A		
A-1	Schematic of the pyrgeometer circuit.	47
A-2	$\delta L_B / (E_O - E_A)$ as a function of temperature.	50
A-3	δL_T as a function of temperature.	52
A-4	Pyrgeometer output as a function of $\sigma(T_d^4 - T_S^4)$.	55
A-5	k values as a function of temperature for downward and upward facing pyrgeometers.	56
A-6	Comparison of corrected and uncorrected pyrgeometer measurements for August 17, 1974, Sabreliner flight. Average for the last two minutes of each leg.	59
A-7	Correction terms as a function of altitude of August 17, 1974, Sabreliner flight.	60
A-8	Infrared heating rates calculated from corrected and uncorrected pyrgeometer measurements.	62
A-9	(a) Uncorrected and (b) Corrected pyrgeometer measurements for July 30, 1974, Sabreliner flight.	65 66
 APPENDIX B		
B-1	DC-6 L+ and H+ measurements. September 7, 1974 1301-1321 GMT.	73

LIST OF FIGURES - Continued

<u>FIGURE</u>		<u>PAGE</u>
B-2	L↓ correction based on difference between dome and sink temperature as a function of H↓. All values are 30 second averages.	74
B-3	Calculated downward LW irradiance for a typical tropical atmosphere and σT_{air}^4 for this same atmosphere.	76
B-4	L↓ as a function of H↓ at points where $\frac{\partial L}{\partial t} \leq 15 \text{ Wm}^{-2} \text{ sec}^{-1}$.	78
B-5	15 second averages of L↓ and H↓ stratified into three separate time intervals.	79
B-6	A plot of $L_{\text{meas}} - aH + \eta$ as a function of $\frac{\partial H}{\partial t}$ for the 1301-1308 time period.	81
B-7	A comparison of corrected and uncorrected L↓ for the September 7, 1974, DC-6 flight.	82

ABSTRACT

This paper presents a description of the basic radiation data gathering systems used on three U.S. Aircraft during the GARP Atlantic Tropical Experiment. In addition to an explanation of the hardware used, the data reduction procedures applied to the raw data are given in detail. Significant problems encountered in the data are also discussed; in some instances remedial steps have been incorporated into the data reduction while in others, the potential user is forewarned about the problems.

1.0 INTRODUCTION

During GATE, the Colorado State University Radiation Project was directly responsible for making radiation measurements from three of the U.S. aircraft - the NOAA C-130, the NOAA DC-6, and the NCAR Sabreliner. Each of these aircraft were equipped with sensors capable of making broadband hemispheric radiation measurements in both the longwave and shortwave portions of the spectrum.

In this report, the radiation measurement systems used on the aircraft are described. A discussion of the calibration of these systems and documentation of the calibration factors and data reduction equations needed to convert raw data to engineering units are included.

In research done prior to GATE, it was shown that the precision of the longwave sensors (pyrgeometers) may be considerably improved by making various temperature corrections on the sensor output (Albrecht et al, 1975). These temperature corrections are considered in detail in this paper and an application of these corrections to the data is discussed.

In the initial data reduction, it became apparent that the downward longwave irradiance measurements of the DC-6 were subject to contamination by shortwave radiation. An investigation of this effect is reported in this study and an empirical correction to the data is suggested.

2.0 DESCRIPTION OF RADIATION MEASUREMENT SYSTEMS

The basic radiation measurement system used on all aircraft (C-130, DC-6, and Sabreliner) is sketched in Fig. 1. It consisted of upward and downward facing shortwave and longwave hemispheric sensors mounted on the top and bottom surfaces of the aircraft. The millivolt output from these sensors was then amplified to a signal level of several volts. The exact voltage range of the amplified signal varied between aircraft and will be discussed below. The amplified signal was then digitized and logged on magnetic tape by the aircraft data logging system. A visual display of the amplified outputs was also available at the observer's station on each aircraft.

The shortwave sensors used on the aircraft were Eppley Precision Pyranometers which have a spectral range of .285 to 2.80 μ . The longwave sensors were Eppley Precision Infrared Radiometers which are sensitive to radiation in the 4-50 μ m spectral range. The amplifiers used to amplify the millivolt signals were Acromag model 311 By-u thermocouple amplifiers.

2.1 U.S. C-130 and DC-6 Systems

Sensors on the U.S. C-130 and DC-6 were mounted on a mechanism which allowed them to be retracted into a "pod" for protection. [Photos of the inside of the pod and the pods mounted on the aircraft are shown in Fig. 2,3 & 4] When mounted on the aircraft, sensors protruding from the pod were 30-45 cm from the skin of the aircraft, which minimized the amount of aircraft surfaces in the field of view of the instruments. The millivolt amplifiers were mounted in the fiberglass nose of the pods.

From the observer's position in each of these aircraft it was possible to monitor the temperature of the inside surface of the pod so that this surface could be used as a calibration target for the retracted

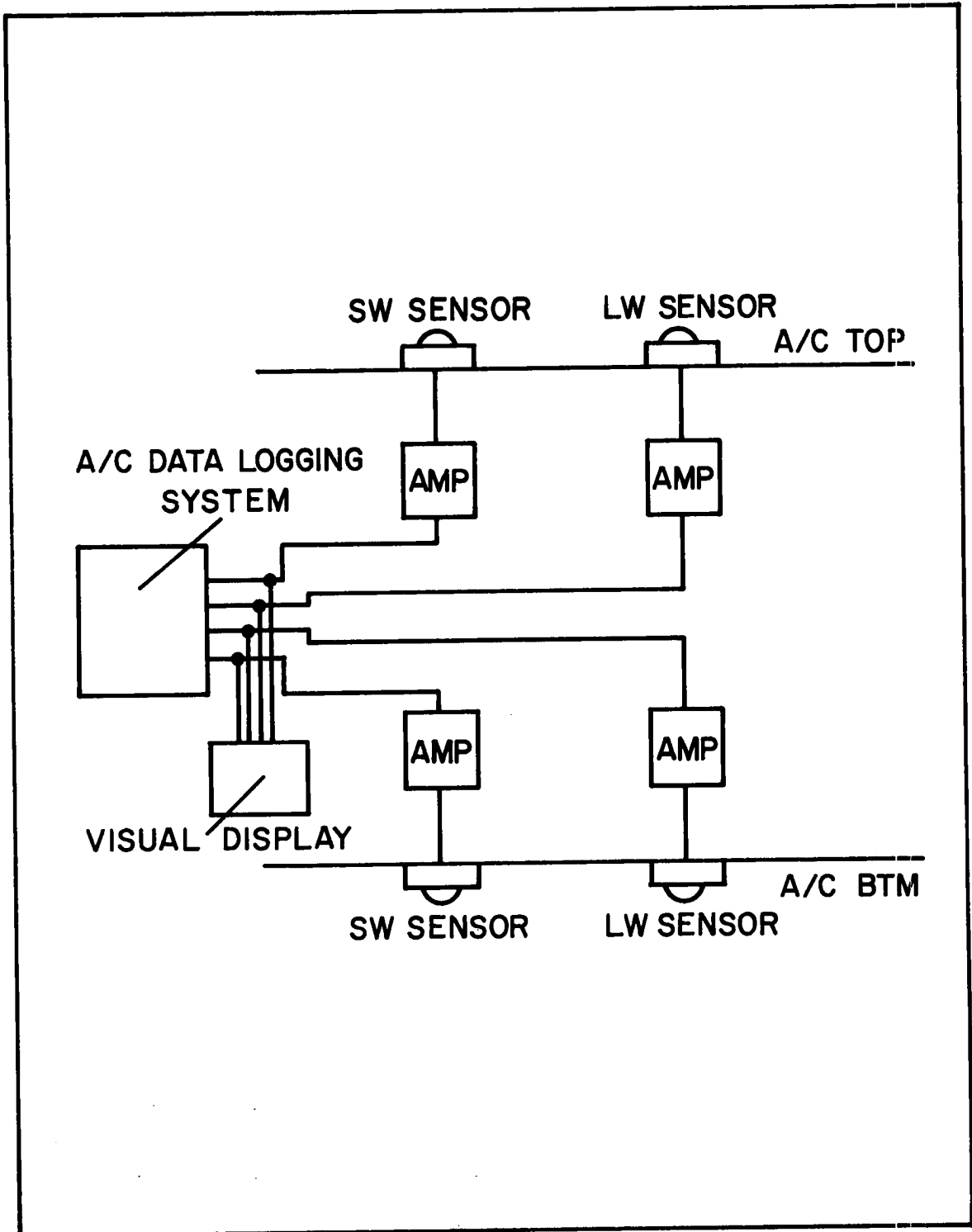


Figure 1. Basic radiation measurement system.



Figure 2. Photograph of inside of pod.



Figure 3. Photograph of pod mounted on DC-6 aircraft.



Figure 4. Photograph of pod mounted on C-130 aircraft.

longwave sensors. Normal operation of the shortwave sensors could also be determined by illuminating these retracted sensors with a small incandescent source. The input of the amplifiers could also be shorted remotely from the observers station so that the zero point offsets of the amplifiers could be determined periodically.

The U.S. C-130 data system had an input range of -10 to +10 volts. Raw data were recorded in terms of counts where 1000 counts is equivalent to 10 volts. The DC-6 data system input range was -5 volts to +5 volts where 5 volts was equivalent to 2027 counts.

2.2 Sabreliner System

Sensors on the NCAR Sabreliner were mounted directly on the skin of the aircraft. The upward facing sensors were mounted on the fuselage while the downward facing sensors were mounted on the lower sides of the wings. Because of the large temperature variations which might be experienced by this aircraft, the millivolt amplifiers and batteries for the longwave sensors were mounted inside the aircraft cabin. The Sabreliner data system input range was -5 to +5 volts. Raw data were recorded in counts where 1000 counts were equivalent to 5 volts.

3.0 THEORY OF OPERATION OF BROADBAND HEMISPHERIC RADIATION SENSORS

3.1 Precision Pyranometer (SW)

The precision pyranometer is described in detail by Robinson (1966). Briefly, this instrument consists of a flat blackened thermopile surface immersed under two concentric quartz glass hemispheres. The instrument has temperature compensation circuitry designed to make the instrument sensitivity nominally constant over a temperature range of -20 to +20°C.

3.2 Precision Infrared Radiometers (LW)

The pyrgeometers used on the U.S. aircraft (C-130, DC-6, Sabreliner, Electra, and Convair 990) were manufactured by Eppley Laboratories. These pyrgeometers were first described by Drummond et al (1970). The theory of their operation and the testing of these instruments from an aircraft platform was described by Albrecht et al (1973).

The Eppley pyrgeometer consists of a thermopile sensor, shielded by a KRS-5 hemisphere. An interference filter is vacuum deposited on the inside of the KRS-5 hemisphere to prevent the transmission of radiation at wavelengths less than 3.5 μm . The thermopile is coated with flat black paint. The sensitivity of the sensor is approximately $.005 \text{ mv/Wm}^{-2}$ with a response time of approximately two seconds.

The longwave radiation, L, is given by the relationship

$$L = \epsilon_0 \sigma T_s^4 + E/\eta - k\sigma(T_d^4 - T_s^4) \quad (1)$$

where ϵ_0 is the emissivity of the thermopile, σ is the Stefan-Boltzman constant, E is the sensor output in mv, η is the sensor sensitivity and k is a constant. T_s is the thermopile cold junction or sink temperature and T_d is the temperature of the KRS-5 hemisphere. The sink temperature T_s is measured with a bead thermistor at the point where the cold junctions are connected to the instrument housing. The dome temperatures for instruments used in GATE

were measured using a small bead thermistor attached to the inside of the KRS-5 hemisphere. A more detailed description of the instrument operation on an aircraft is given in Appendix A.

3.21 Precision Infrared Radiometer Laboratory Calibration Procedure

The precision infrared radiometers (pyrgeometers) were calibrated using a conical cavity blackbody of large thermal mass. Various target temperatures were obtained by cooling the blackbody to approximately -10°C and allowing the blackbody to warm as the calibrations were performed. Blackbody temperatures were measured at several points on the surface of the conical aperture using thermocouples attached to this surface. Temperature differences between these points were found to be less than $.2^{\circ}\text{C}$.

To determine the sensitivity of the Eppley thermopile, the instrument was faced into the blackbody cavity while thermopile output, sink temperature and dome temperature were recorded as a function of time for approximately five minutes at each calibration point. An example of instrument output and the dome and sink temperatures as a function of time are shown in Fig. 5 for a calibration point. Initially the KRS-5 dome was warmer than the sink, however, when the instrument was faced into the blackbody, the dome cooled quickly as it lost energy to the cold blackbody; at the same time the thermopile sink cooled much more slowly since its thermal mass is much greater. After approximately three minutes the dome and sink cooled at approximately the same rate. The instrument output initially decreased rapidly and then stabilized after approximately three minutes. This behavior is consistent with Eq. (1) which may be written in the form

$$\frac{E}{\eta} = L - \epsilon_0 \sigma T_s^4 + k\sigma(T_d^4 - T_s^4). \quad (2)$$

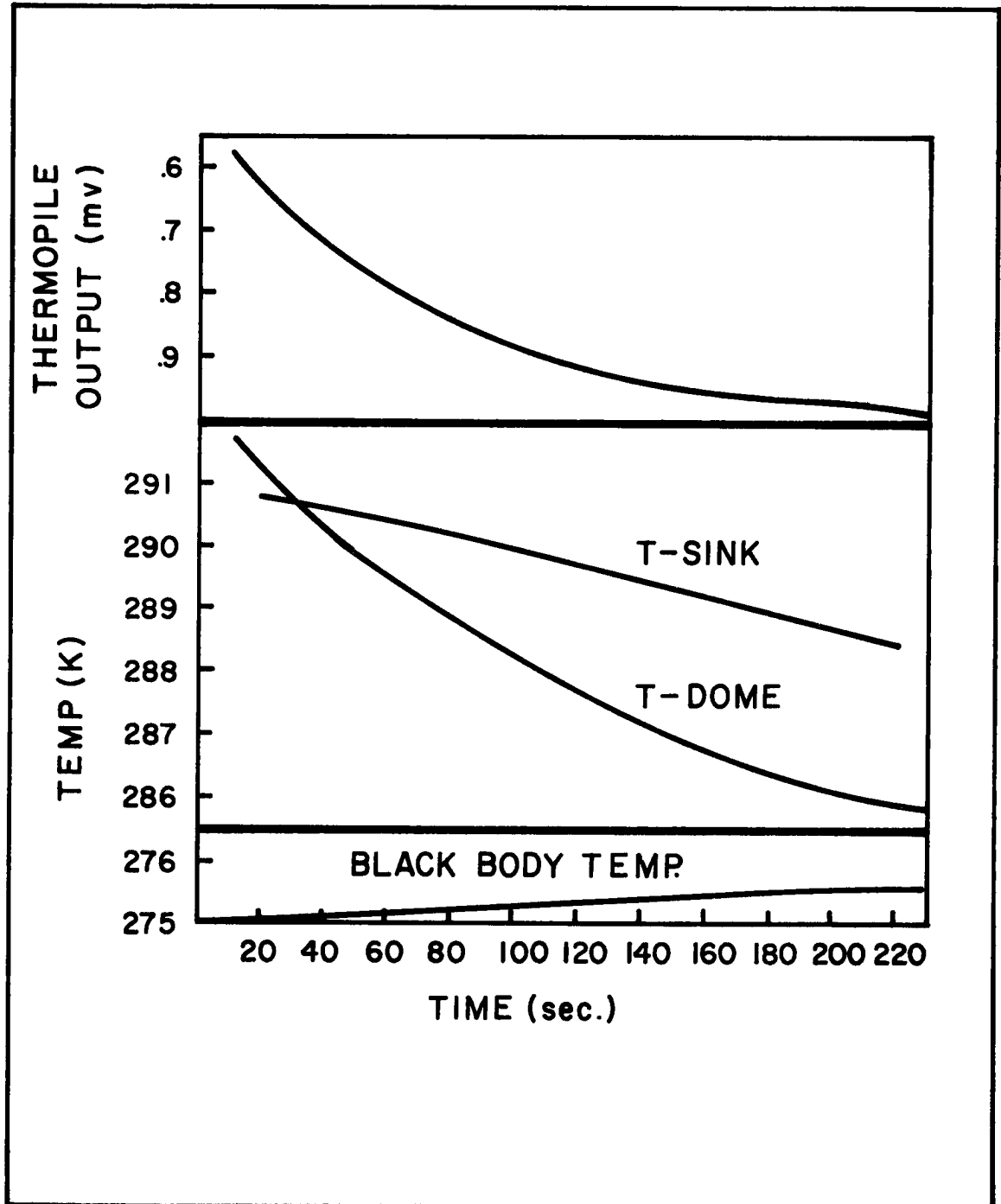


Figure 5. Variation of dome and sink pyrgometer temperatures as a function of time during a blackbody calibration.

The dominance of the $k\sigma(T_d^4 - T_s^4)$ is apparent in the variation of output as a function of time as shown in Fig. 5.

To determine n in Eq. (2), the instrument output, E , at points where $T_d = T_s$ is plotted against $L - \epsilon_0\sigma T_s^4$ where L in this case is determined by the blackbody temperature. In the results given here, the emissivity of both the blackbody and the thermopile are assumed to be 1.0. A plot of these points is shown in Fig. 6. The slope of the line connecting these points gives $\frac{1}{n} = 178 \text{ Wm}^{-2}\text{mv}^{-1}$.

The k value in Eq. (4) may then be determined by plotting $\sigma(T_d^4 - T_s^4)$ as a function of $L - \epsilon_0\sigma T_s^4 - \frac{E}{n}$ assuming the sensitivity determined in the procedure described above. Plots for three of the runs are shown in Fig. 7. The average value of k determined from these plots is $k = 4.08$.

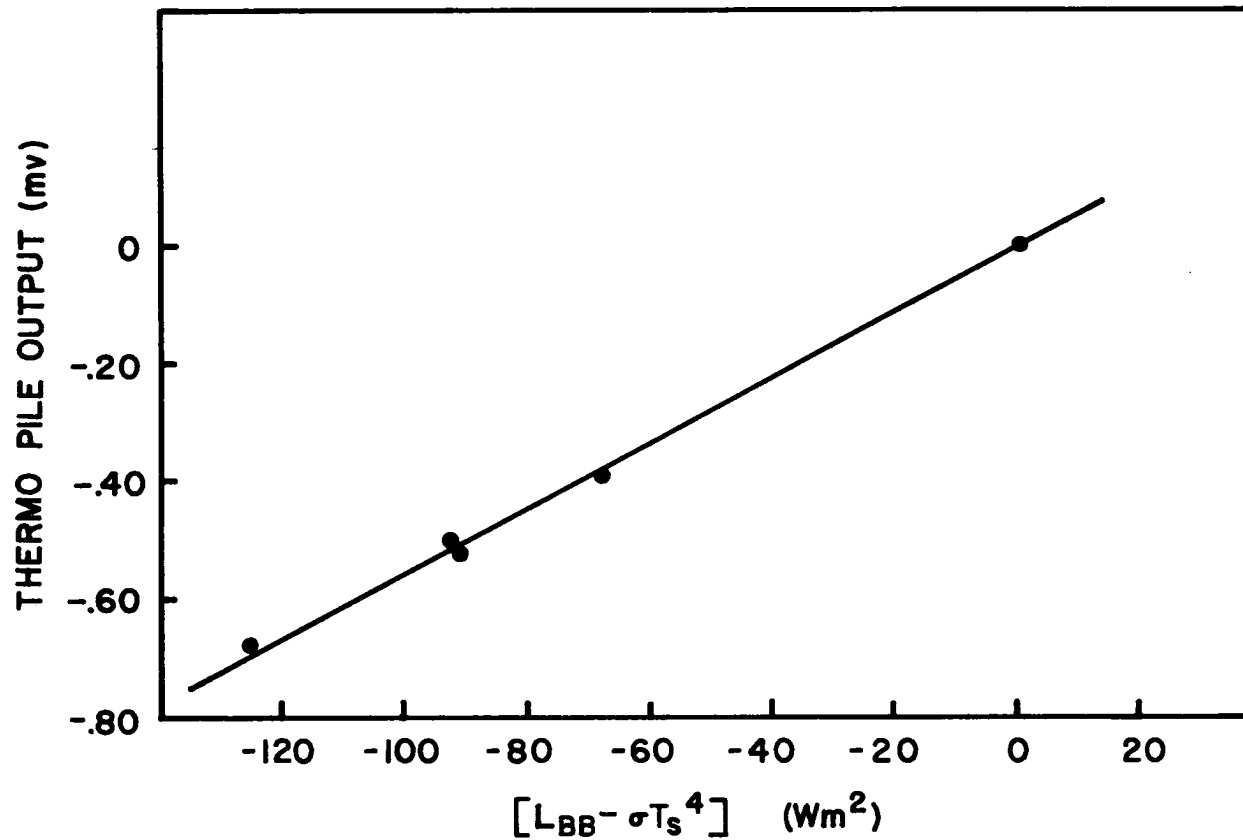


Figure 6. Thermopile output as a function of the difference in the radiative energy per unit area emitted by the blackbody and the thermopile surface.

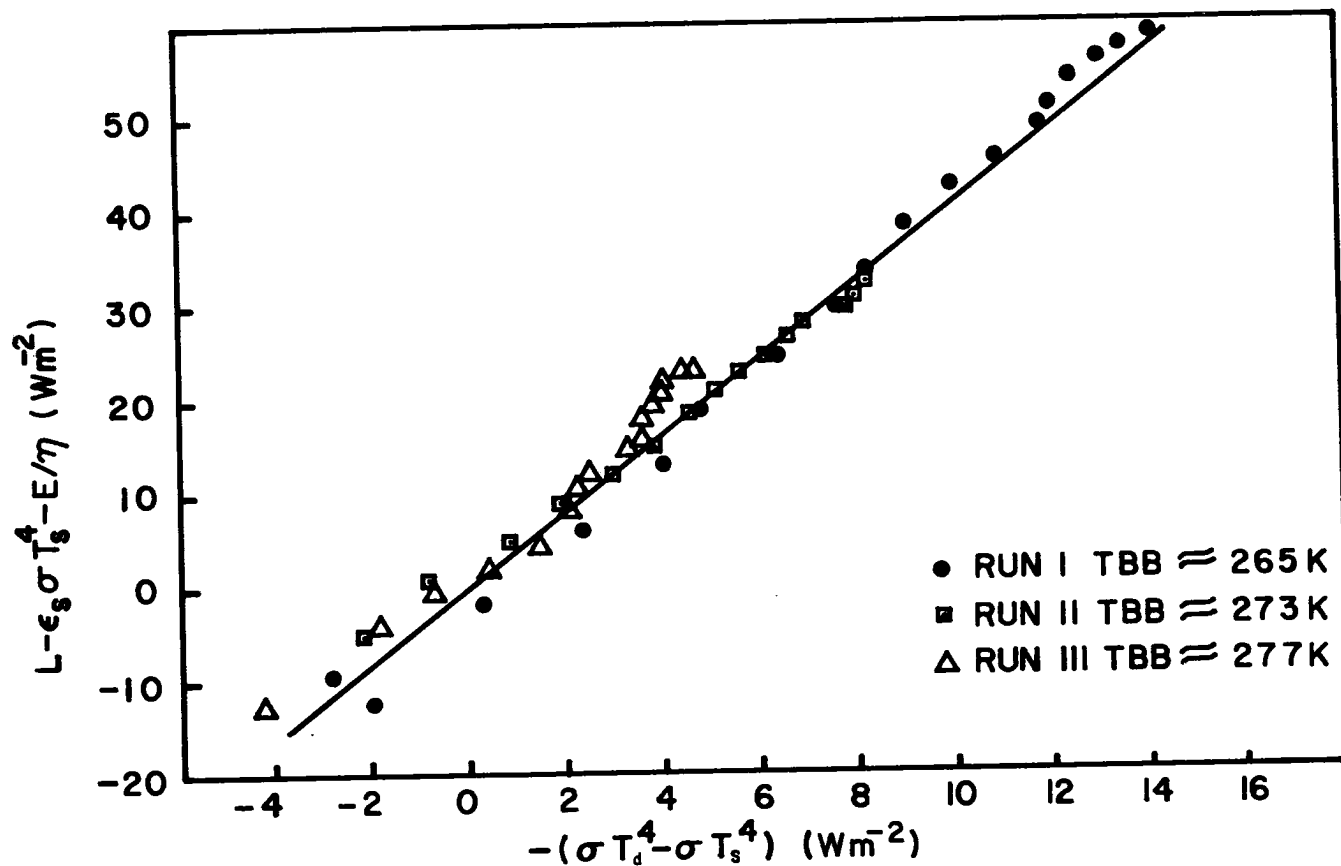


Figure 7. $L - \epsilon_s \sigma T_s^4 - E/\eta$ as a function of $(\sigma T_d^4 - \sigma T_s^4)$. The coefficient k is given by the slope of these points. T_{bb} is the approximate blackbody temperature at each calibration point.

4.0 CALIBRATION AND DATA REDUCTION

4.1 Sensors

Each aircraft measures four basic irradiance values. The parameters and the coding that will be used to designate each are given below.

L↓ - LW downward irradiance

L↑ - LW upward irradiance

H↓ - SW downward irradiance

H↑ - SW upward irradiance

Initial sensor calibrations were performed by Eppley Laboratories. One point calibration checks were also made periodically during the experiment using a simple black body cone. A final calibration check was made at Colorado State University after the conclusion of the experiment.

4.2 Amplifier / Data System Calibrations

Amplifiers and data systems were calibrated simultaneously. A Leads and Northrop potentiometer was used to provide varying millivolt signals to the input of the mv amplifiers. The resulting amplifier outputs were then recorded on magnetic tape. Hence, an exact relationship between input voltages and the recorded output was determined.

4.3 First Order Data Reduction Equation Factors

The instrument calibrations and amplifier calibrations were combined to define a relationship which may be used to convert data system values into irradiance values. It was found that this relationship was a linear function to within the uncertainty of the calibration procedure. Hence, the irradiance is given as $\text{irradiance} = ax - b$, where x represents data system counts and a and b are determined by the calibrations described

above. The factors a and b varied slightly during the experiment since instruments were occasionally interchanged or replaced. In general, however, the variations in a and b due to variations in amplifier performance were small. Some gradual variations in b were observed during the experiment. These variations, however, may in many cases be easily corrected for since zero point calibrations were typically made several times during each flight. After the calibration factors have been applied to the data, any non-zero offset values simply define additive factors needed to correct the data.¹ The calibration factors for the U.S. Sabreliner, C-130 and DC-6 are listed in Tables I- III.

¹ It has been noted that the offsets determined by the inflight shorting of the amplifier inputs increase or decrease in time due to a heating of the relay contacts used to short the input. Consequently, only the first several seconds of amplifier shorts should be used to make an additional refinement on the radiation data.

PARAMETER	DATA SYSTEM ID	DAYS EFFECTIVE	a	b
L↓	Cox 1	172-220	1.03000	165.83
L↓	Cox 1	221-231	1.02576	167.19
L↓	Cox 1	232-262	1.10566	182.44
L↑	Cox 3	172-180	1.10566	162.54
L↑	Cox 3	181-231	1.10566	165.84
L↑	Cox 3	232-262	1.03815	156.77
H↓	Cox 2	172-262	2.53380	401.17
H↑	Cox 4	172-201	1.66241	266.13
H↑	Cox 4	202-262	1.66869	267.41

Table I. Calibration factors for US C-130.

$$y = ax - b$$

where y is irradiance in Wm^{-2} and x is data system counts.

PARAMETER	DATA SYSTEM ID	DAYS EFFECTIVE	a	b
L↓	Cox 19	172-201	.53275	176.82
L↓	Cox 19	202-231	.53257	177.87
L↓	Cox 19	232-262	.53240	177.59
L↑	Cox 21	172-201	.50021	169.60
L↑	Cox 21	202-231	.49826	169.44
L↑	Cox 21	232-262	.49664	167.56
H↓	Cox 20	172-201	.98434	322.91
H↓	Cox 20	202-262	.98434	318.59
H↑	Cox 22	172-179	.86699	289.91
H↑	Cox 22	180-194	.43888	146.56
H↑	Cox 22	195-201	.43888	147.48
H↑	Cox 22	202-214	.44117	148.28
H↑	Cox 22	215-231	.44117	152.63
H↑	Cox 22	232-262	.44278	153.19

Table II. Calibration factors for US DC-6.

$$y = ax - b$$

where y is irradiance in Wm^{-2} and x is data system counts.

PARAMETER	DATA SYSTEM ID	DAYS EFFECTIVE	a	b
L↓	D1	197-240	1.27395	243.34
L↓	D1	241-262	1.36936	261.56
L↑	F1	197-217	1.37062	259.23
L↑	F1	218-240	1.36685	263.00
L↑	F1	241-262	1.26811	243.51
H↓	D4	197-217	2.02802	385.24
H↓	D4	218-238	2.02802	386.23
H↓	D4	239-262	2.02802	387.34
H↑	D6	197-217	1.56393	294.00
H↑	D6	218-238	1.56290	294.72
H↑	D6	238-262	1.56188	295.24

Table III. Calibration factors for NCAR Sabreliner

$$y = ax - b$$

where y is irradiance in Wm^{-2} and x is data system counts.

4.4 Higher Order Corrections Applied to Data Reduction

In a previous section, we have given a simple linear relation between irradiance and voltage output of the sensor. However, as noted in the theory of operation of the instruments (Section 3.0) there are higher order corrections which may be applied to further refine the data. These higher order corrections are summarized below.

4.5 Corrections to SW Data

4.51 Geometry Correction for Non Horizontal Sensor

Although pyranometer mounts were carefully leveled relative to the center line of the aircraft, the aircraft normally flies at an angle of from three to fifteen degrees from the horizontal depending primarily on air speed, altitude and fuel load and distribution. At small solar zenith angles encountered at local noon in low latitudes, this problem is minimized, however at larger zenith angles encountered prior to 10 a.m. and after 2 p.m. LST the problem may become quite severe. If one assumes that the incident irradiance is dominated by the direct component, a geometrical correction may be made using the following formula.

$$I_o = I_p [\cos \epsilon (\sin \phi \sin \delta + \cos \phi \cos \delta \cos \tau) + \sin \epsilon \{ \cos A_p [\tan \phi (\sin \phi \sin \delta + \cos \phi \cos \delta \cos \tau) - \sin \delta \sec \phi] + \sin A_p \cos \delta \sin \tau \}]^{-1}$$

where I_p is the irradiance measured by the inclined sensor
 I_o is the irradiance on a horizontal surface
 ϵ is the angle of inclination of the sensor above the plane of the horizontal (aircraft pitch angle)
 ϕ is the latitude of the aircraft
 δ is the solar declination
 τ is the solar hour angle

A_p is the azimuthal heading of the aircraft

The derivation of this equation may be found in Robinson (1966).

4.52 Temperature Correction

Although the Eppley precision pyranometer does have temperature compensating circuitry, this circuitry only approximately maintains a linear relationship over a large temperature range.

4.521. Sabreliner

Corrected values of H_{\downarrow} and H_{\uparrow} for the Sabreliner were determined from the following expressions:

$$H_{\downarrow}(\text{corr}) = H_{\downarrow} * K_3(T) \quad (3)$$

$$H_{\uparrow}(\text{corr}) = H_{\uparrow} * K_4(T) \quad (4)$$

In the above expressions, H_{\downarrow} and H_{\uparrow} are irradiances resulting from the first order data reduction equation given in section 4.3. The temperature dependent functions $K_3(T)$ and $K_4(T)$ given in Tables IV and V were determined from laboratory measurements. The temperature, T , used to make this correction was total air temperature.

4.522. NOAA C-130

Corrected values of H_{\downarrow} and H_{\uparrow} for the C-130 were determined from the expressions

$$H_{\downarrow}(\text{corr}) = H_{\downarrow} * K_5(T) \quad (5)$$

$$H_{\uparrow}(\text{corr}) = H_{\uparrow} * K_6(T) \quad (6)$$

where $K_5(T)$ and $K_6(T)$ are given in Table VI and VII.

4.523. NOAA DC-6

Corrected values of H_{\downarrow} and H_{\uparrow} for the DC-6 were determined from the expressions:

Temperature °C	K_3
-70	1.047
-60	1.030
-50	1.015
-40	1.004
-30	0.997
-20	0.994
-10	0.996
0	1.000
10	1.006
20	1.017

Table IV. K_3 as a function of temperature for use in calculating H_+ (corr).
Instrument Serial No. 12515F3
Top Sabreliner Pyranometer.

Temperature °C	K_4
-70	1.073
-60	1.056
-50	1.040
-40	1.024
-30	1.013
-20	1.006
-10	1.002
0	1.000
10	1.002
20	1.006

Table V. K_4 as a function of temperature
for use in calculating $H_t(\text{corr})$.
Instrument Serial No. 12514F3
Bottom Sabreliner Pyranometer

Temperature °C	K_5
-70	---
-60	---
-50	---
-40	1.022
-30	1.011
-20	1.005
-10	1.002
0	1.000
10	1.000
20	1.002

Table VI. K_5 as a function of temperature
for use in calculating $H_{\uparrow}(\text{corr})$.
Instrument Serial No. 12512F3
Top C-130 pyranometer

Temperature °C	K_6
-70	---
-60	---
-50	---
-40	1.007
-30	1.001
-20	0.998
-10	0.998
0	1.000
10	1.006
20	1.017

Table VII. K_6 as a function of temperature
for use in calculating $H^{\dagger}(\text{corr})$.
Instrument Serial No. 12517F3
Bottom C-130 pyranometer.

$$H (\text{corr}) = H * K_7(T) \quad (7)$$

$$H (\text{corr}) = H * K_8(T) \quad (8)$$

where $K_7(T)$ and $K_8(T)$ are given in Table VIII and IX.

4.6 Corrections to the LW Data

The theory of operation of the pyrgeometer is given in section 3.2. The paragraphs below explain how these corrections were applied to specific aircraft.

4.61 Sabreliner

In the first order LW data reduction, one depends upon electronic circuitry to approximate the effects of the terms shown analytically in Eq. 1. Considerable improvement in the instrument performance may be achieved if these terms are evaluated analytically. In the following paragraphs, the data reduction procedures used to incorporate analytically the effects of the self emission of the thermopile and the dome-sink temperature differences are explained. The following equations were used to make the corrections.

$$L_{\uparrow}(\text{corr}) = K_1(L_{\uparrow} - L_B) + 1.327 \times 10^{-7}UST^4 - 7.654 \times 10^{-8}UDT^4 \quad (9)$$

$$L_{\uparrow}(\text{corr}) = K_2(L_{\uparrow} - L_B) + 1.327 \times 10^{-7}DST^4 - 7.654 \times 10^{-8}DDT^4 \quad (10)$$

where L_{\uparrow} and L_{\downarrow} are the resultant irradiances from the first order data reduction (section 4.3). A detailed description of the corrections given in Eq. 5 and 6 is given in Appendix A. The variables UST, UDT, DST and DDT are defined in Table XIV. L_B is the self emission of the thermopile and is determined from the battery voltage, E_0 , given in Table X as a function of Julian Day and from Table XI which gives L_B/E_0 as a function of temperature (UST, DST).

Temperature °C	K_7
-70	---
-60	---
-50	---
-40	1.012
-30	1.007
-20	1.002
-10	1.000
0	1.000
10	1.004
20	1.011

Table VIII. K_7 as a function of temperature
for use in calculating H_+ (corr).
Instrument Serial No. 12516F3
Top DC-6 pyranometer

Temperature °C	K_8
-70	---
-60	---
-50	---
-40	1.014
-30	1.008
-20	1.003
-10	1.002
0	1.000
10	1.001
20	1.005

Table IX. K_8 as a function of temperature
for use in calculating $H\uparrow(\text{corr})$
Instrument Serial No. 12513F3
Bottom DC-6 pyranometer.

DAY	BATTERY VOLTAGE E_0 VOLTS
210-227	1.350
228	1.500
229	1.490
230	1.483
231	1.475
232, 233	1.466
234, 235	1.456
236, 237	1.447
238, 239	1.436
240, 241	1.426
242, 243	1.416
244, 245	1.407
246, 247	1.398
248, 249	1.389
250, 251	1.380
252, 253	1.372
254, 255	1.366
256-262	1.360

Table X Sabreliner battery voltage
as a function of Julian Day.

INSTRUMENT TEMPERATURE	L_B/E_0 ($Wm^{-2}/volt$)
35	378.00
25	333.14
15	287.63
5	245.50
-5	209.91
-15	182.21
-25	162.27
-35	148.90
-45	140.44
-55	135.38
-65	132.52

Table XI Sabreliner L_B/E_0 as a function of instrument temperature.

The factors K_1 and K_2 are given in Tables XII and XIII as a function of temperature (UST, DST) and correct for the variation of instrument sensitivity with temperature. The temperature parameters described in Table XIV were converted from raw data to temperatures by using the conversion formula.

$$T(^{\circ}\text{K}) = (c_1 + c_2 \ln R_x + c_3 (\ln R_x)^2)^{-1} \quad (11)$$

where $R_x = 45.0 \left(\frac{1092}{\text{aris counts}} - 1 \right)$

$$c_1 = .2741984 \times 10^{-2}$$

$$c_2 = .2539640 \times 10^{-3}$$

$$c_3 = .5176294 \times 10^{-5}$$

4.62 NOAA C-130 Self Emission Correction

In addition to the four parameters L_{\downarrow} , L_{\uparrow} , determined in the first generation procedure, two parameters, $L_{\downarrow}(\text{corr})$ and $L_{\uparrow}(\text{corr})$ were included in the reduced parameters. These parameters are given by the equations

$$L_{\downarrow}(\text{corr}) = L_{\downarrow} + \delta L_T \quad (12)$$

$$L_{\uparrow}(\text{corr}) = L_{\uparrow} + \delta L_T. \quad (13)$$

δL_T is identical for each instrument and depends only on instrument temperature (total air temperature for the DC-6 and C-130). The δL_T correction accounts for the deviation between the actual emission of the thermopile surface ($\epsilon_0 \sigma T_S^4$ in Eq. 1) and the signal produced by the internal circuitry of the Eppley pyrgeometer. A detailed description of this correction is given in Appendix A. The dependence of δL_T on temperature is given in Table XV. δL_T has units of Wm^{-2} identical to the units of L_{\downarrow} and L_{\uparrow} . Since δL_T will generally vary slowly with time, it need not be redetermined any more frequently than once every 15 seconds.

TEMPERATURE (°C)	K_1
-70	1.067
-60	1.040
-50	1.020
-40	1.009
-30	1.003
-20	1.000
-10	0.999
0	1.000
10	1.006
20	1.014

Table XIIa. For use in calculating $L_+(CORR)$
for Julian Days 197 through 240 only.
 K_1 as a function of temperature.
Instrument Serial No. 12504F3
Top Sabreliner Pyrgeometer

TEMPERATURE (°C)	K_1
-70	1.063
-60	1.045
-50	1.028
-40	1.011
-30	1.004
-20	1.000
-10	0.999
0	1.000
10	1.004
20	1.010

Table XIIb For use in calculating $L_+(CORR)$
for Julian Days 241 through 262 only.
 K_1 as a function of temperature.
Instrument Serial No. 12506F3
Top Sabreliner Pyrgeometer

Temperature °C	K ₂
-70	1.063
-60	1.045
-50	1.028
-40	1.011
-30	1.004
-20	1.000
-10	0.999
0	1.000
10	1.004
20	1.010

Table XIIIa For use in calculating L+(CORR)
for Julian Days 197 through 240 only.
K₂ as a function of temperature.
Instrument Serial No. 12506F3
Bottom Sabreliner Pyrgeometer

Temperature °C	K_2
-70	1.067
-60	1.040
-50	1.020
-40	1.009
-30	1.003
-20	1.000
-10	0.999
0	1.000
10	1.006
20	1.014

Table XIIIb For use in calculating $L_+(CORR)$
for Julian Days 241 through 262 only.
 K_2 as a function of temperature
Instrument Serial No. 12504F3
Bottom Sabreliner Pyrgeometer

PARAMETER	DESCRIPTION	ARIS LOCATION
UST	Temperature of top pyrgeometer sink	B2
UDT	Temperature to top pyrgeometer dome	D8
DST	Temperature of bottom pyrgeometer sink	G1
DDT	Temperature of bottom pyrgeometer dome	H1

Table XIV Four additional channels on the Sabreliner used to record the temperature of the dome and sink of the LW sensors.

TABLE XV

δL_T AS A FUNCTION OF TEMPERATURE

TEMPERATURE (°C)	δL_T
35	-5.5
25	-4.7
15	0
5	5.8
-5	7.5
-15	4.0
-25	-5.8
-35	-20.2
-45	-37.2
-55	-55.3
-65	-73.3

4.63 NOAA DC-6

In addition to a self emission correction, some solar heating of the KRS-5 dome was detected from the data. Dome temperature measurements during part of the experiment were used to develop an empirical relationship between solar irradiance and a dome heating correction.

4.631 Self Emission Correction

The terms $L_{\downarrow}(\text{corr})$ and $L_{\uparrow}(\text{corr})$ described above also need to be determined for the DC-6 data. The equations for these parameters are similar to those used above. (See section 4.632 for an explanation of the origin of the 20 Wm^{-2} bias applied to L_{\downarrow} in Eq. 14.) I.e.,

$$L_{\downarrow}(\text{corr}) = L_{\downarrow} + \delta L_T - 20.0 \quad (14)$$

$$L_{\uparrow}(\text{corr}) = L_{\uparrow} + \delta L_T. \quad (15)$$

δL_T is determined from total air temperature and Table XV.

4.632 Solar Heating of the DC-6 Pyrgeometer KRS-5 Dome

The effect of the solar heating of the dome may be minimized by applying the following additive correction to the $L_{\downarrow}(\text{corr})$ value given in Eq. 14:

$$\delta L_i = -.0311 H_{i\downarrow} + .0666 \frac{(H_{i\downarrow} - H_{i-2\downarrow})}{2.0} + 20.0 \quad (16)$$

where $H_{i\downarrow}$ is the solar irradiance at the i^{th} second. A detailed derivation of this relationship is given in Appendix B. The coefficients in Eq. 16 are equally valid if Eq. 16 is averaged over some time interval.

For averages over sufficiently large time intervals, the term $.0666 \frac{(H_{i\downarrow} - H_{i-2\downarrow})}{2.0}$ may be ignored. The $+20.0$ term in Eq. 16 results from a constant bias of -20.0 Wm^{-2} applied to all longwave downward DC-6 data (see Eq. 14). The purpose of this bias was to eliminate in an average sense some of the uncertainty due to solar heating of the dome. The -20.0 Wm^{-2} term

corresponds to a constant solar irradiance of approximately 640 Wm^{-2} . It should be noted that this bias was also applied to the offset values discussed in Section 4.3.

5.0 CONCLUDING REMARKS

The scrupulous user of the broadband radiation data from the DC-6, C-130 and Sabreliner aircraft should be able to reconstruct all data reduction steps from the information compiled in this report. This information has been taken from many different sources and is spread over a time interval from two years prior to GATE to the present, 18 months after the GATE field phases.

An overall evaluation of the success of this program will not come until these data are subjected to the detailed scrutiny of scientific users. However, at this point in time, we feel that the data do, in general, offer sufficient variety and quality for application to a number of important and timely scientific problems. This does not by any means imply that the data are perfect for we have pointed out some specific problems and there are probably other problems which will be discovered by future users.

Table XVI lists the presently known problems with the broadband hemispheric aircraft data. These entries fall into three categories: 1) the problem has been identified and a solution implemented and incorporated in the data reduction; 2) the problem has been noted and a solution has been proposed, however, not incorporated into the data reduction and 3) the problem has been noted; however, there is no suggested remedy (NSR) given at this time. The type 2) entries in Table XVI are footnoted.

	PYRANOMETER		PYRGEOMETER				GENERAL	
	SOLAR GEOMETRY	TEMPERATURE DEPENDENCE	WET BULBING	SELF EMISSION	SOLAR CONTAMINATION	DOME-SINK TEMPERATURE DIFFERENCE	AMPLIFIER ZERO DRIFT	RADIO FREQUENCY INTERFERENCE
DC-6	4.51 +	4.52	NRS	4.631 App A	4.632 + App B	App B +	4.3 +	NRS
C-130	4.51 +	4.52	NRS	4.62 App A			4.3 +	NRS
SABRELINER	4.51 +	4.52	NRS	4.61 App A		App A	4.3 +	NRS

Table XVI Listing of aircraft broadband radiation data problems noted to date. Where a suggested remedy exists the appropriate section of this report outlining the remedy is given. + indicates that these procedures have not been incorporated into the data reduction procedures. Where a problem has been noted but no remedy has been suggested, the abbreviation NRS is used.

ACKNOWLEDGEMENTS:

Many individuals and many organizations deserve thanks in recognition of the roles they have played in experiment design, hardware design, data collection and data reduction for the U.S. DC-6, C-130 and Sabreliner radiation experiments. We shall mention a few key individuals by name and readily admit that there are many other unnamed individuals who made significant contributions to the success of the experiment.

Dr. James McFadden and the entire staff of the NOAA RFF graciously supported our efforts throughout the experiment. Special thanks is also offered to the NCAR Research Aircraft Facility for their support both prior to and during the experiment. Pilots Loyd Newcomer and Pete Orum and technician Ron Ruth gave our experiments exceptional attention and support throughout the experiment. Mr. Al Miller and the NCAR GADMAP group have been exceptionally patient as we have made every attempt to optimize the quality of the radiation data from these aircraft. Their willingness to cooperate in an iterative manner with us during the data reduction phase has resulted in a much higher quality radiation data set for scientific consumption than would have been otherwise available.

To Drs. Douglas Sargeant and James Rasmussen and their staff at the NOAA GATE project office and to Drs. Eugene Bierly and Richard Greenfield of the NSF, we offer our sincere gratitude for the confidence they displayed in our ability to acquire a high quality aircraft radiation data set. Without the support of these people prior to, during and after the GATE field phase, our accomplishments would have been significantly fewer in number.

We gratefully acknowledge the support by the Global Atmospheric Research Program, National Science Foundation and the GATE Project Office, NOAA.

APPENDIX A

TEMPERATURE CORRECTED AIRCRAFT PYRGEOMETER MEASUREMENTS

by
B. A. Albrecht
and S. K. Cox

Department of Atmospheric Science
Colorado State University
Fort Collins, Colorado
80523

TABLE OF CONTENTS

	<u>PAGE</u>
A-I. INTRODUCTION	45
A-II. PYRGEOMETER PERFORMANCE: THEORETICAL VS. ACTUAL	46
A-III. PYRGEOMETER CORRECTIONS	49
A. Battery Voltage Uncertainties	49
B. Non-Linearity of Pyrgeometer Temperature Compensation Circuitry	51
C. Dome-Sink Temperature Differences	53
A-IV. APPLICATION OF CORRECTIONS TO REAL DATA	58
A-V. CONCLUSIONS AND RECOMMENDATIONS	67
REFERENCES	69

<u>FIGURE</u>	LIST OF FIGURES	<u>PAGE</u>
A-1	Schematic of the pyrgeometer circuit.	47
A-2	$\delta L_B / (E_O - E_A)$ as a function of temperature.	50
A-3	δL_T as a function of temperature.	52
A-4	Pyrgeometer output as a function of $\sigma(T_d^4 - T_s^4)$.	55
A-5	k values as a function of temperature for downward and upward facing pyrgeometers.	56
A-6	Comparison of corrected and uncorrected pyrgeometer measurements for August 17, 1974, Sabreliner flight. Average for the last two minutes of each leg.	59
A-7	Correction terms as a function of altitude for August 17, 1974, Sabreliner flight.	60
A-8	Infrared heating rates calculated from corrected and uncorrected pyrgeometer measurements.	62
A-9	(a) Uncorrected and (b) Corrected pyrgeometer measurements for July 30, 1974, Sabreliner flight.	65 66

A.I. INTRODUCTION

The Eppley Laboratories pyrgeometer is an instrument designed to measure hemispheric radiation in the 4-50 μ spectral range. Although this sensor was originally intended to be used in a ground station configuration, pyrgeometer measurements have been successfully made from aircraft (Albrecht, et al, 1974; abbreviated A74). During GATE, Eppley pyrgeometers were mounted on five of the U.S. aircraft participating in that experiment.

Under certain circumstances, pyrgeometer measurements made from aircraft may be more precise than those made from a ground station installation. This is particularly true for daytime measurements when the solar load on the sensor is large (A74). In the ground station installation, the KRS-5 hemisphere of the instrument is heated by the solar radiation. This heating results in erroneously high outputs. When mounted on an aircraft, the increased air flow tends to minimize the effect of the solar heating.

In other instances, however, the extreme temperature variations experienced by the sensors mounted on aircraft may degrade the precision of the pyrgeometer measurements. This is particularly true for sensors mounted on aircraft capable of flying at very high altitudes.

In this paper, the systematic errors which may be encountered in aircraft pyrgeometer measurements are explored and techniques are developed to correct these measurements. The techniques developed are used to correct a real data set. The magnitude of each correction term is considered and the effect of these corrections on the infrared heat budgets is discussed.

A.II. PYRGEOMETER PERFORMANCE: THEORETICAL VS. ACTUAL

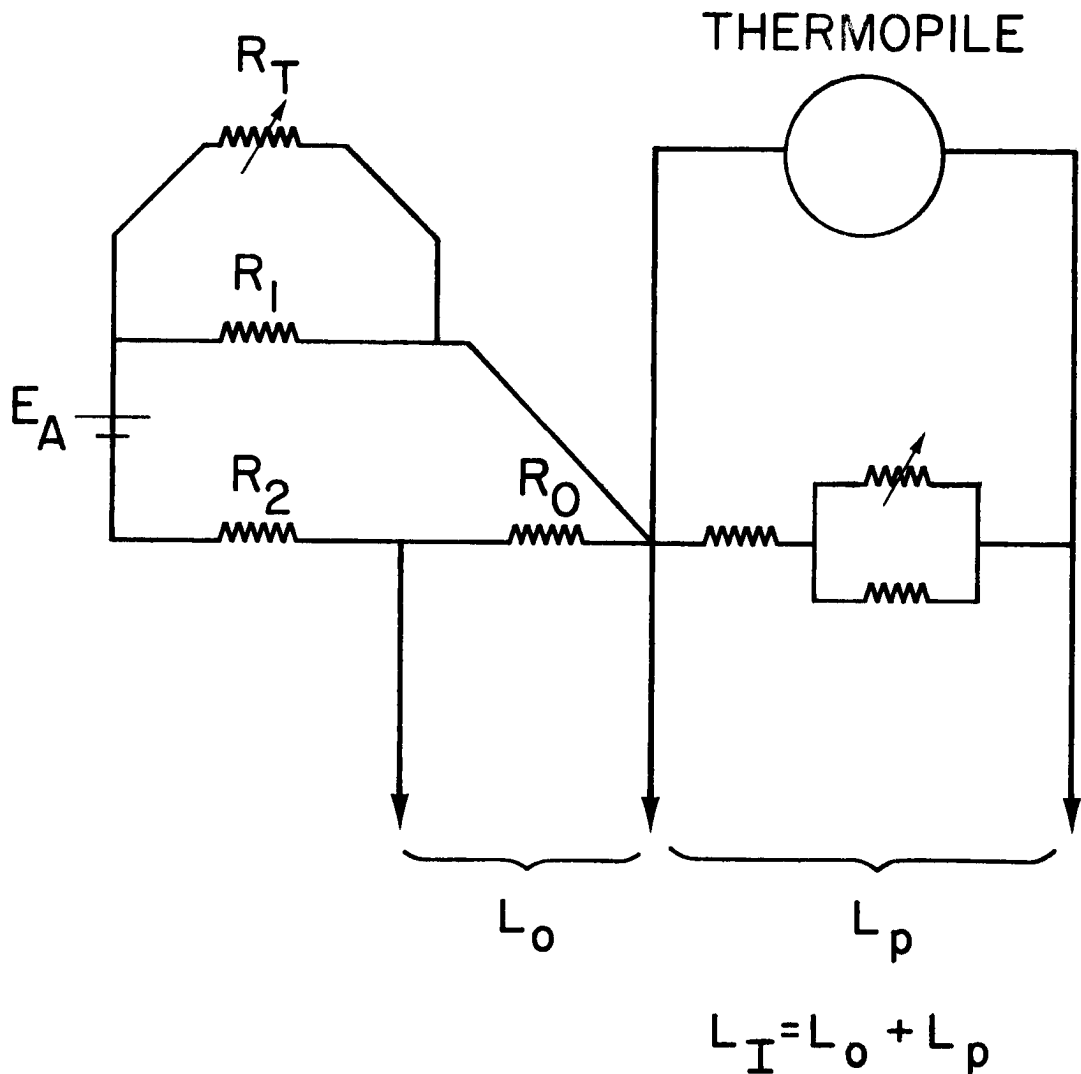
The pyrgeometer consists of a thermopile enveloped by a KRS-5 hemisphere. An interference filter is vacuum deposited on the inside of the hemisphere. By accurately specifying the heat budget of the sensor, the radiation incident upon the sensor may be expressed in terms of thermopile output and sensor temperatures. In A75, a heat budget relationship was derived for the Eppley pyrgeometer which may be written as

$$L = L_{\text{net}}(c_1 + c_2 T_s^3) + \epsilon_0 \sigma T_s^4 - k\sigma(T_d^4 - T_s^4) \quad (1)$$

where L is the incident irradiance, L_{net} is net radiation at the thermopile surface, T_s is the temperature of the thermopile cold junction (referred to as the sink temperature) and T_d is the temperature of the KRS-5 hemisphere; ϵ_0 is the emissivity of the thermopile surface, σ is the Stefan-Boltzman constant and k is a constant which may be experimentally determined.

In actuality, the Eppley pyrgeometer uses thermistor-resistor networks to represent the T_s^3 and T_s^4 dependencies indicated in Eq. (1). The constants c_1 , c_2 and ϵ_0 are determined implicitly when the instrument is calibrated. Calibrations are made, however, with $T_d = T_s$; hence, the last term in Eq. (1) is not considered. It should be noted, however, that in actual operation nothing guarantees that T_d will equal T_s .

The internal pyrgeometer circuitry used to account for the temperature dependencies in the first two terms on the right hand side of Eq. (1) is shown in Fig. A-1. The left hand side of the circuit is the circuit used to approximate the $\epsilon_0 \sigma T_s^4$ term. The right hand side of the circuit is the temperature compensated thermopile output and represents $L_{\text{net}}(c_1 + c_2 T_s^3)$. Since $c_1 \gg c_2 T_s^3$ for all temperatures and $L_{\text{net}}(c_1 + c_2 T_s^3)$ is less than $\epsilon_0 \sigma T_s^4$, temperature corrections in the term $L_{\text{net}}(c_1 + c_2 T_s^3)$ will be small compared to other corrections and will not be considered at this time.



TYPICAL RESISTANCE VALUES

$$R_T = 10 \text{ K}\Omega @ 25^\circ\text{C}$$

$$R_1 = 35.8 \text{ K}\Omega$$

$$R_2 = 9.97 \text{ K}\Omega$$

$$R_0 = 35.4 \text{ K}\Omega$$

$$K_0 = 166.9 \text{ Wm}^{-2}\text{mv}^{-1}$$

Figure A-1. Schematic of the pyrgeometer circuit.

There are at least two possible circumstances when the left-hand side of the circuit shown in Fig. A-1 does not accurately produce a signal equivalent to the $\epsilon_0 \sigma T_s^4$ term. The first is due to uncertainties in the battery voltage E. The second is the inability of the circuit to reproduce the T_s^4 dependence over a large range of temperatures.

As indicated above, the pyrgeometer circuitry makes no attempt to approximate the $k\sigma(T_d^4 - T_s^4)$ term in Eq. (1). For sensors mounted on an aircraft, there are several situations when this term may be significant. This is particularly true immediately after ascent or descent to a different level. The KRS-5 dome in these cases will respond quickly to the temperature variations, but the remainder of the instrument responds much more slowly. Even after several minutes of flight at a particular level, there may be compressional differential heating of the instrument. Hence, a temperature difference between dome and sink may even exist as a steady state condition.

If Eq. (1) is considered to be an accurate representation of the pyrgeometer's heat budget, the actual irradiance L may be written in terms of the actual instrument output as

$$L = L_I + \delta L_B + \delta L_T + \delta L_{DS} \quad (2)$$

L_I in this equation is the uncorrected instrument output, δL_B is a correction for differences between actual battery voltage, E, and some standard voltage, E_0 . δL_T is a correction for the non-linearity between the battery circuit output (L_0) and $\epsilon_0 \sigma T_s^4$ and $\delta L_{DS} = -k\sigma(T_d^4 - T_s^4)$. In the following, each of the correction terms in Eq. (2) will be considered in detail to determine their magnitudes and dependence on sensor temperature.

A.III. PYRGEOMETER CORRECTIONS

A. Battery Voltage Uncertainties

The voltage, E_A , shown in Fig. A-1 is supplied by a small mercury cell mounted inside the instrument. Although the voltage of the mercury cells used are generally quite stable, small variations in this voltage may result in large variations in the pyrgeometer output.

Referring to the left-hand side of Fig. 1, it is evident that

$$\delta L_B = \frac{(E_0 - E_A)(k_0 R_0)}{R_{T1} + R_2 + R_0}, \quad (3)$$

where E_0 is some standard voltage, ($E_0 = 1.35$ volts), k_0 is the instrument sensitivity, and

$$R_{T1} = \frac{R_1 R_T}{R_1 + R_T}. \quad (4)$$

Typical values of $\delta L_B / (E_0 - E_A)$ calculated from Eq. (3) are shown in Fig. A-2. It is apparent that the largest absolute errors due to the battery voltage uncertainty occur at warmer temperatures. The relationship shown in Fig. A-2 indicates that a .10 volt variation in the battery voltage will result in a 33 Wm^{-2} variation in instrument output at 25°C . The variations become absolutely smaller at colder temperatures, although the relative variation may be as large.

During GATE, the pyrgeometer batteries were mounted in the cabin of the NCAR Sabreliner aircraft to prevent battery failure at low temperatures. The voltages of the mercury cells varied from 1.50 to 1.35 volts during the experiment. Although the cells used for these pyrgeometers did not appear to be as stable as those typically used in the instrument, these variations will result in an error of 45 Wm^{-2} at 25°C .

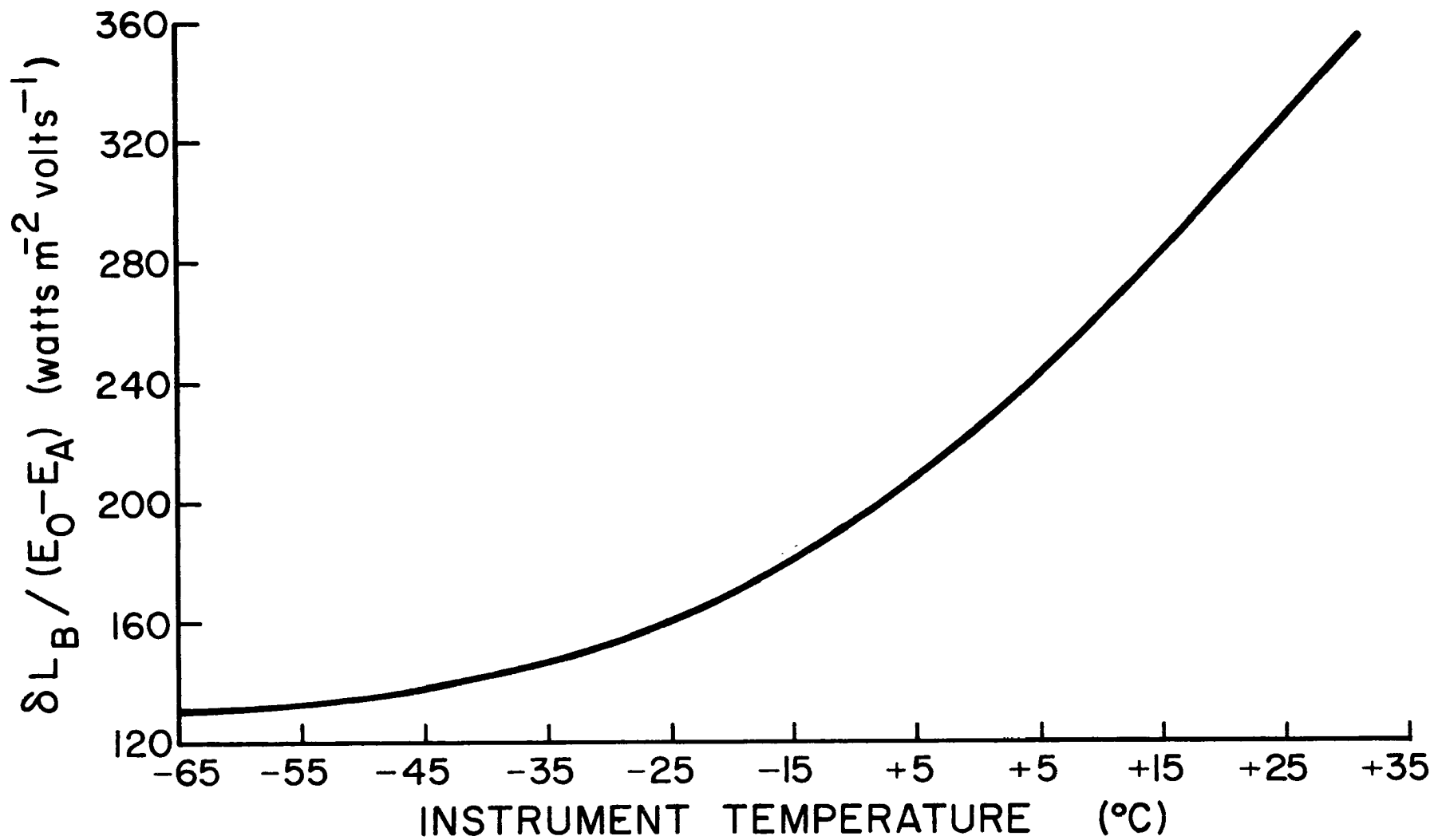


Figure A-2. $\delta L_B / (E_0 - E_A)$ as a function of temperature.

B. Non-Linearity of Pyrgeometer Temperature Compensation Circuitry

To determine the errors introduced by the non-linearity of the battery circuit, the term $\epsilon_0 \sigma T_s^4$ in Eq. (1) is compared to the corresponding output of the instrument. Using Eq. (3), this may be written as

$$\delta L_T = \epsilon_0 \sigma T_s^4 - (E_0 k_0 R_0) / (R_{T1} + R_2 + R_0) \quad (5)$$

The emissivity, ϵ_0 , of the thermopile surface is approximately 1.0. To determine an exact value for ϵ_0 , it was assumed that $\delta L_T = 0$ at 15°C, the temperature at which sensor sensitivities were determined by Eppley.

Values of δL_T calculated using Eq. (5) are shown in Fig. A-3 as a function of cold junction temperature. For temperatures between 30°C and -25°C, the value of δL_T is less than $\pm 8 \text{ Wm}^{-2}$. However, at temperatures less than -25°C, the value of $|\delta L_T|$ increases rapidly with decreasing temperature.

The δL_T errors at low temperatures are not only large in the absolute sense, but may be extremely large in the relative sense. Consider, for example, a hypothetical case in which the actual downward longwave irradiance is 70 Wm^{-2} at a temperature level of -55°C and 80 Wm^{-2} at -45°C. If it is assumed that the thermopile output of the instrument is correct at both levels, the actual instrument output would be 125 Wm^{-2} at -55°C and 117 Wm^{-2} at -45°C. Not only are these values in error by more than 40 Wm^{-2} , the irradiance measured by the sensor actually increases with height. This increase of irradiance with height was observed on the NCAR Sabliner during GATE when legs were flown at 11.9 km and 13.1 km respectively. It is important to note, however, that if both the upward and downward facing sensors are at the same temperature, the δL_T correction will not affect the net irradiance at a level.

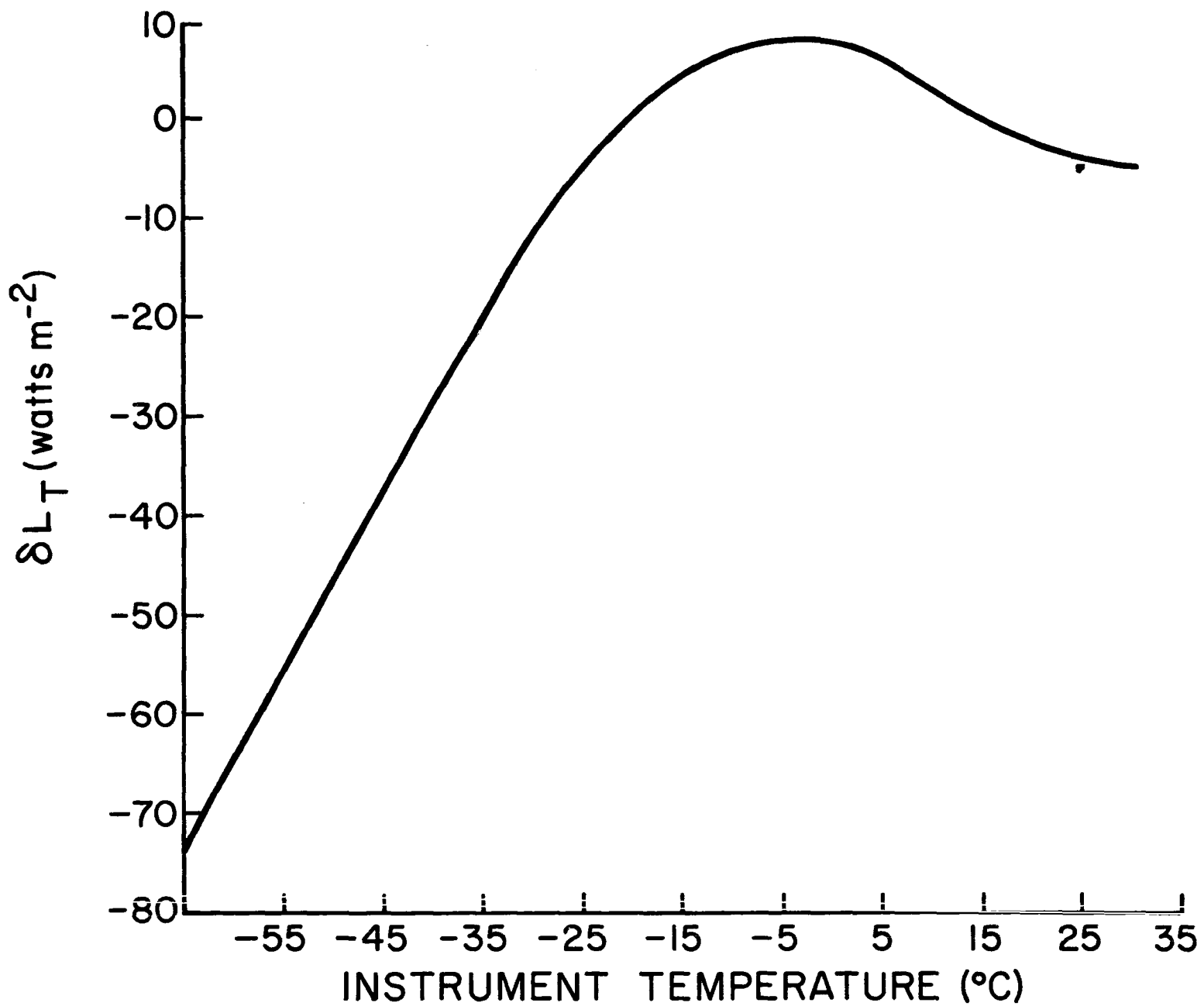


Figure A-3. δL_T as a function of temperature.

C. Dome-Sink Temperature Differences

To determine the magnitude of the term $k\sigma(T_d^4 - T_s^4)$ it is necessary to make independent measurements of T_d and T_s . It is not obvious, however, how the dome temperature T_d should be determined, since the temperature may not be constant over the entire dome.

The instruments used on the Saberliner had a small bead thermistor attached to the inside of the KRS-5 hemisphere. The temperature determined at this single point may be significantly different than the average dome temperature. However, if variations in this temperature are representative of the average temperature variations of the dome, the $k\sigma(T_d^4 - T_c^4)$ relationship should be maintained with the proper choice of k .

An attempt was made to determine the constant k from a real data set. The particular data used was collected during a NCAR Saberliner flight made on August 17, 1974, approximately 320 km off the coast of Senegal, West Africa. During this flight, a uniform stratocumulus deck with a top at approximately .9 km was observed. Haze to 4.73 km and some high cirrus were also reported. The flight consisted of 19 constant pressure altitude legs, each of a duration of approximately four minutes. The legs were flown at altitudes of 9.45 km to 15 m above the sea surface.

The NCAR Saberliner was equipped with both upward and downward facing pyrgeometers during GATE. The millivolt outputs from these instruments were amplified to a 0-5 volt range and were recorded on magnetic tape at a sampling rate of four per second. Dome and sink temperatures were determined using thermistors mounted within the instrument and were also recorded on magnetic tape.

To determine k at a particular level, it is assumed that the infrared target viewed by the instrument is constant. The output of the instrument

(corrected for δL_B and δL_T errors) is then correlated linearly with $\sigma(T_d^4 - T_s^4)$. The slope of the linear relationship between the instrument output determines k , as shown for example in Fig. A-4.

The results shown in Fig. A-4 were determined at a constant pressure level of 45.3 kPa using the upward facing sensor. The temperature at this level was -10.4°C and was preceded by a descent from a level of 28.8 kPa and -33°C . Consequently, since the sink temperature responds slowly to this temperature change, $T_d > T_s$ during the entire leg. The difference between T_d and T_s decreases with time. The linear fit at this level is excellent with k having a value of 3.67. Only values every fifteen seconds are shown in Fig. A-4. At all levels and for both instruments, a similar analysis was performed using values averaged over three second intervals.

The 3.67 value for k shown in Fig. A-4 is significantly greater than the 1.35 value of k reported in A75 under laboratory conditions. Values of k determined at other temperatures are shown in Fig. A-5. In a few cases the k values shown in Fig. A-5 were determined subjectively. This was done when instrument output variations were obviously due to variations in the infrared target. In other cases, no clear linear trend was discernable and k values could not be determined. This was particularly true for flight levels made in the vicinity of the stratus or when $T_d \simeq T_s$ during the entire leg.

The values of k for the downward facing sensor (Fig. A-5) compare favorably with the laboratory value of 1.35. The value at -33°C , however, is significantly larger than 1.35, although the variation of $T_d - T_s$ was small for this case.

The values of k for the upward facing sensor varies from 1.0-1.8 for temperatures warmer than 0°C . However, at temperature colder than 0°C , the

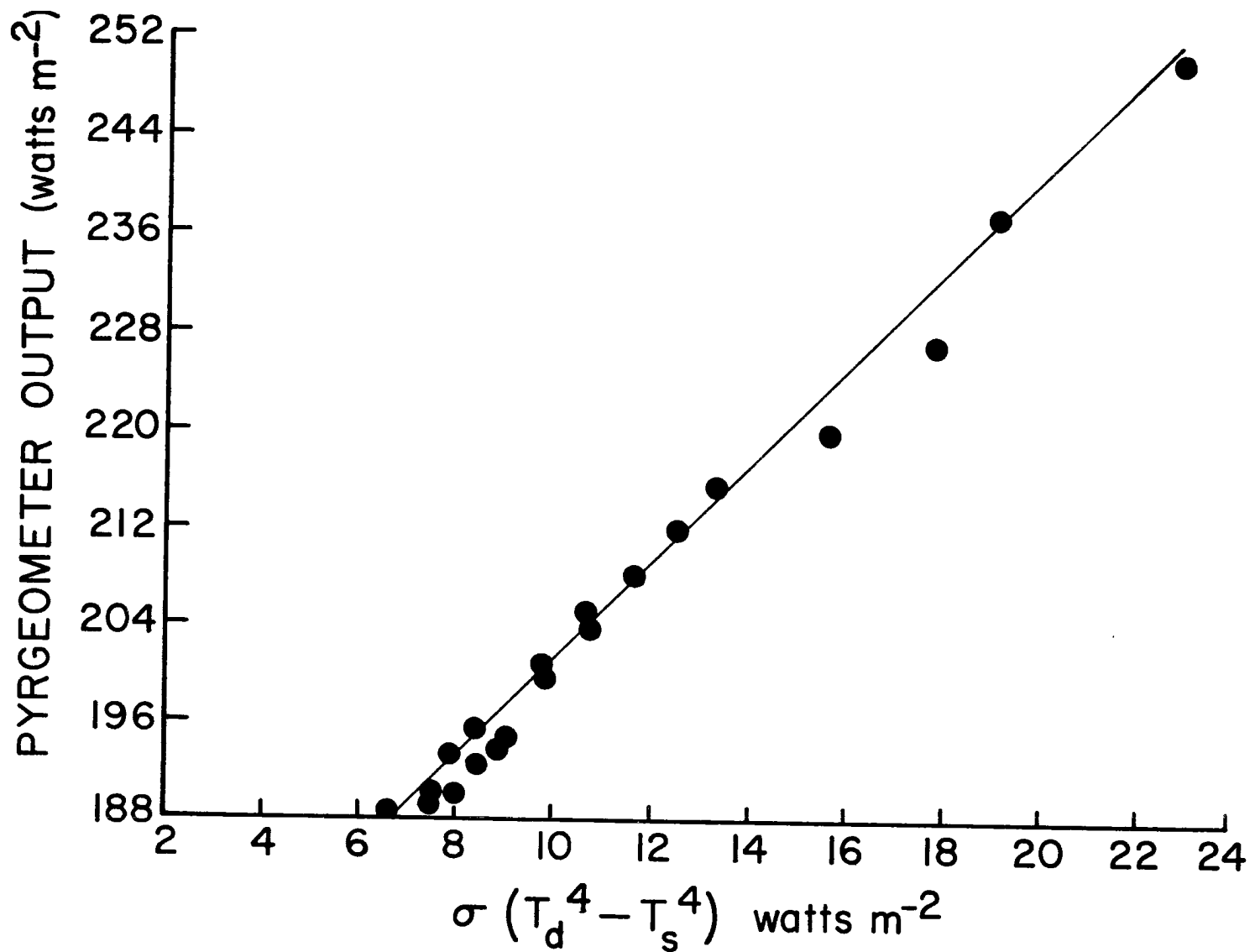


Figure A-4. Pyrgometer output as a function of $\sigma(T_d^4 - T_s^4)$.

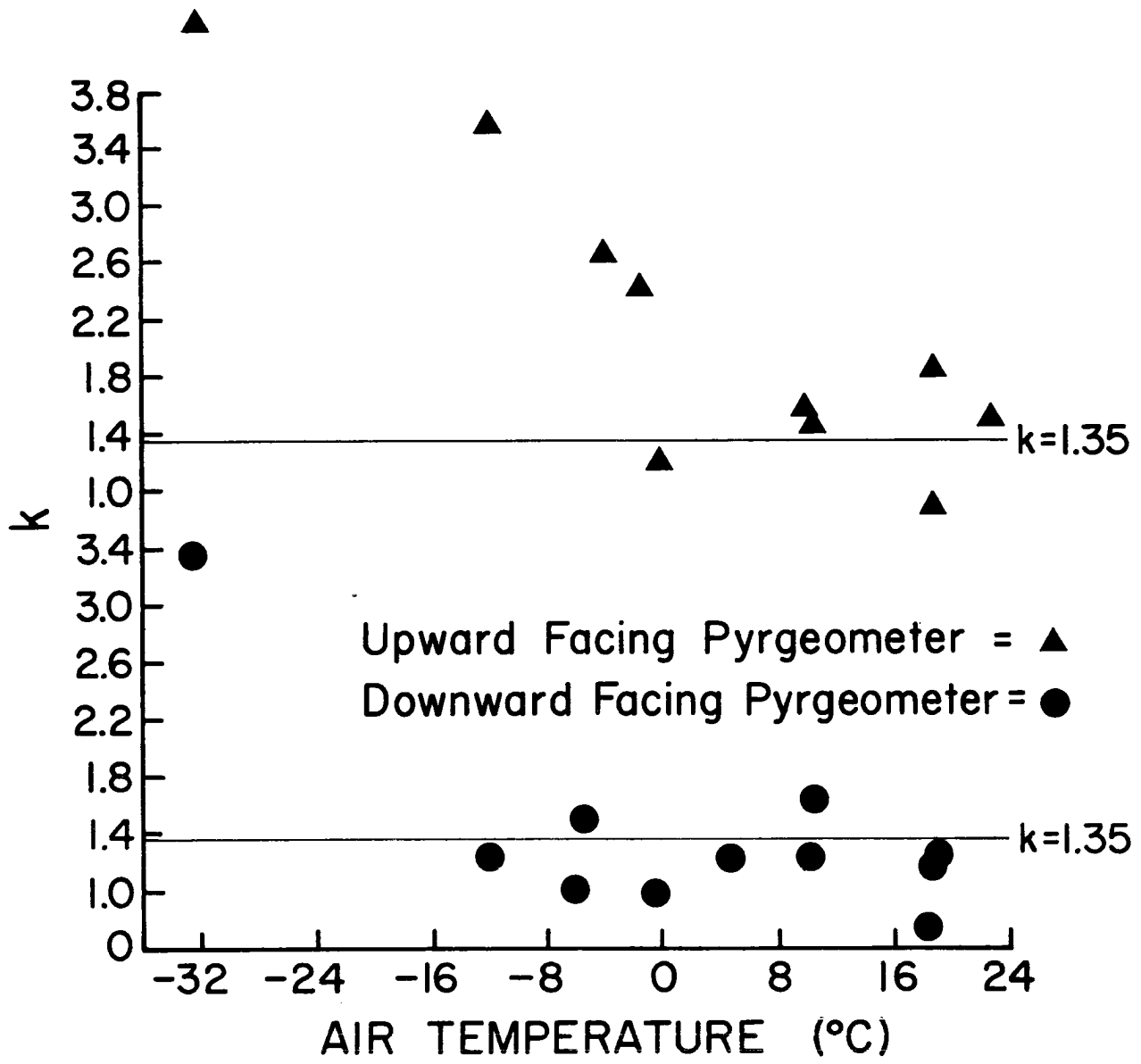


Figure A-5. k values as a function of temperature for downward and upward facing pyrometers.

k values appear to increase with decreasing temperatures to a value approximately three times as great as the laboratory value. Unfortunately, the data in this single flight is not sufficient to confidently establish any relationships between k and instrument temperature. In the future, additional data will be investigated to determine k values at cold temperatures. During GATE, several flights were made during clear sky conditions. Although these data are not presently available, they should prove to be very useful in establishing the variations in k as determined by the single point dome temperature measurements.

A.IV. APPLICATION OF CORRECTIONS TO REAL DATA

The temperature corrections described above were applied to a real data set. The flight considered was flown on August 17, 1974 and is the same flight used previously to determine the value of k in the δL_{ds} correction term. The pyrgeometer battery voltages needed to make the δH_B corrections were measured to be 1.49 volts for both the upward and downward facing sensor. The corrections were performed using three second averages of uncorrected pyrgeometer outputs and thermistor measurements. The k needed to make the δL_{ds} correction was assumed to be 1.35.

The downward irradiance (measured by the upward facing pyrgeometer) averaged over the last two minutes of each leg is shown in Fig. A-6 for both the corrected and uncorrected data. The average leg was approximately four minutes long. As indicated in Fig. A-6, the corrected and uncorrected values differ by as much as 80 Wm^{-2} at 30.0 kPa. These differences decrease to approximately 30 Wm^{-2} at 300 mb.

The flight made on August 17 actually consists of two separate profiles, each made in a descending mode. The agreement shown in Fig. A-6 between the measurements made during each profile is excellent even though cloud cover was not absolutely uniform.

The magnitudes of the individual correction terms averaged over the last two minutes of each leg are shown as a function of pressure in Fig. A-7 for Run I. The δL_B term accounts for a large portion of the correction since battery voltages were relatively large on this flight. The large differences at low levels are almost totally due to this high voltage. The correction δL_{ds} resulting from temperature differences between the dome and sink difference has an average value of $10\text{-}12 \text{ Wm}^{-2}$.

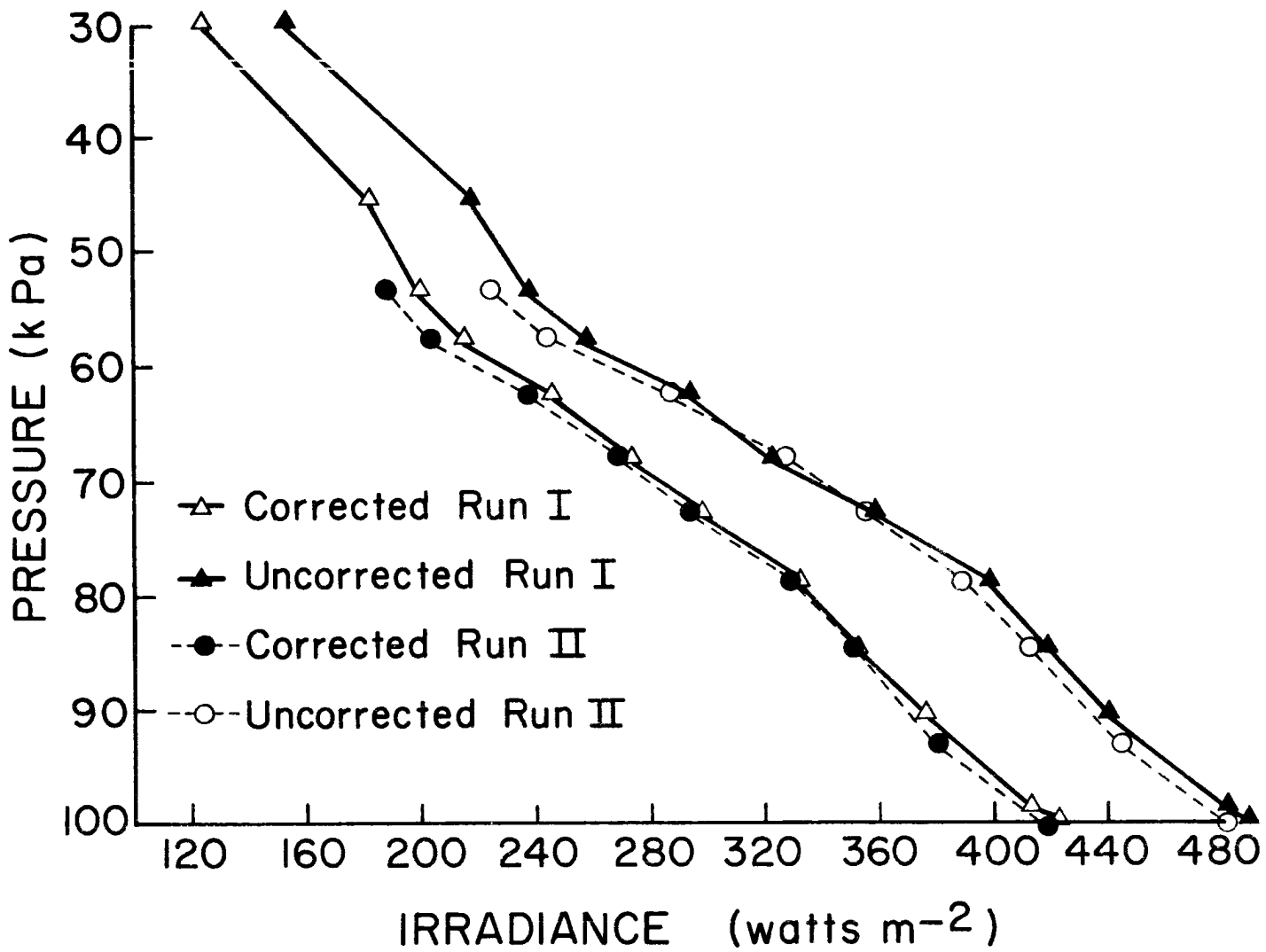


Figure A-6. Comparison of corrected and uncorrected pyrgometer measurements of L_{\downarrow} for August 17, 1974, Sabreliner flight. Average for the last two minutes of each leg.

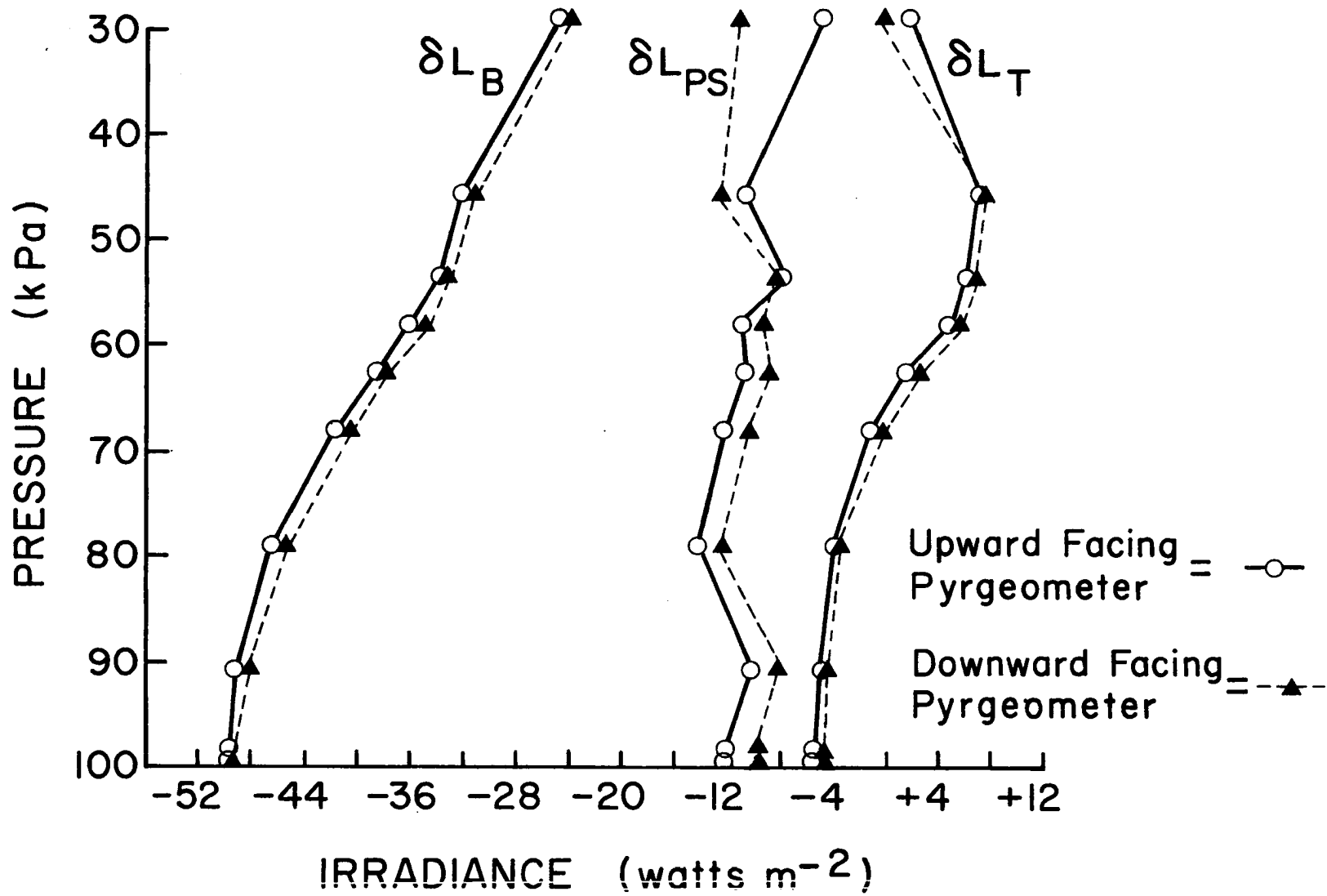


Figure A-7. Correction terms as a function of altitude for August 17, 1974, Sabreliner flight.

This results from the dome having a slightly warmer steady state temperature than the sink of the instrument. The correction for the non-linearity of the pyrometer circuit averages $\pm 4 \text{ } \mu\text{m}^{-2}$. Although this is a relatively small correction, it may be, as shown by Fig. A-3, much greater for flights made at very cold temperatures.

The correction terms for the downward facing pyrometer are shown in Fig. A-7. These corrections are nearly identical to the corrections for the upward facing instrument. Consequently, the infrared heating rate calculated from the corrected and uncorrected data should not be significantly different. It should be noted, however, that the correction values shown in Fig. A-7 represent steady state values since these values are the average value over the last two minutes. Heating rates calculated from corrected and uncorrected data may differ if the instruments are not in thermal equilibrium.

The infrared heating rates calculated from the corrected and uncorrected irradiance values are shown in Fig. A-8. As indicated by the variations of the correction terms in Fig. A-7, the heating rates for the corrected and uncorrected data do not differ significantly except at higher altitudes. At the higher levels, the differences are $\sim .4^{\circ}\text{C day}^{-1}$, while below 55 kPa, the differences are $< .1^{\circ}\text{C day}^{-1}$. The infrared heating rates for Run II are not shown here. During that portion of the flight, condensation in the external connector of the downward facing instrument provide a conductive path between the millivolt output of the instrument and the thermistor connections.

As shown in A75, the dome-sink correction term may be useful in eliminating the errors which occur before dome-sink temperatures stabilize following ascents and descents. To demonstrate this, the difference

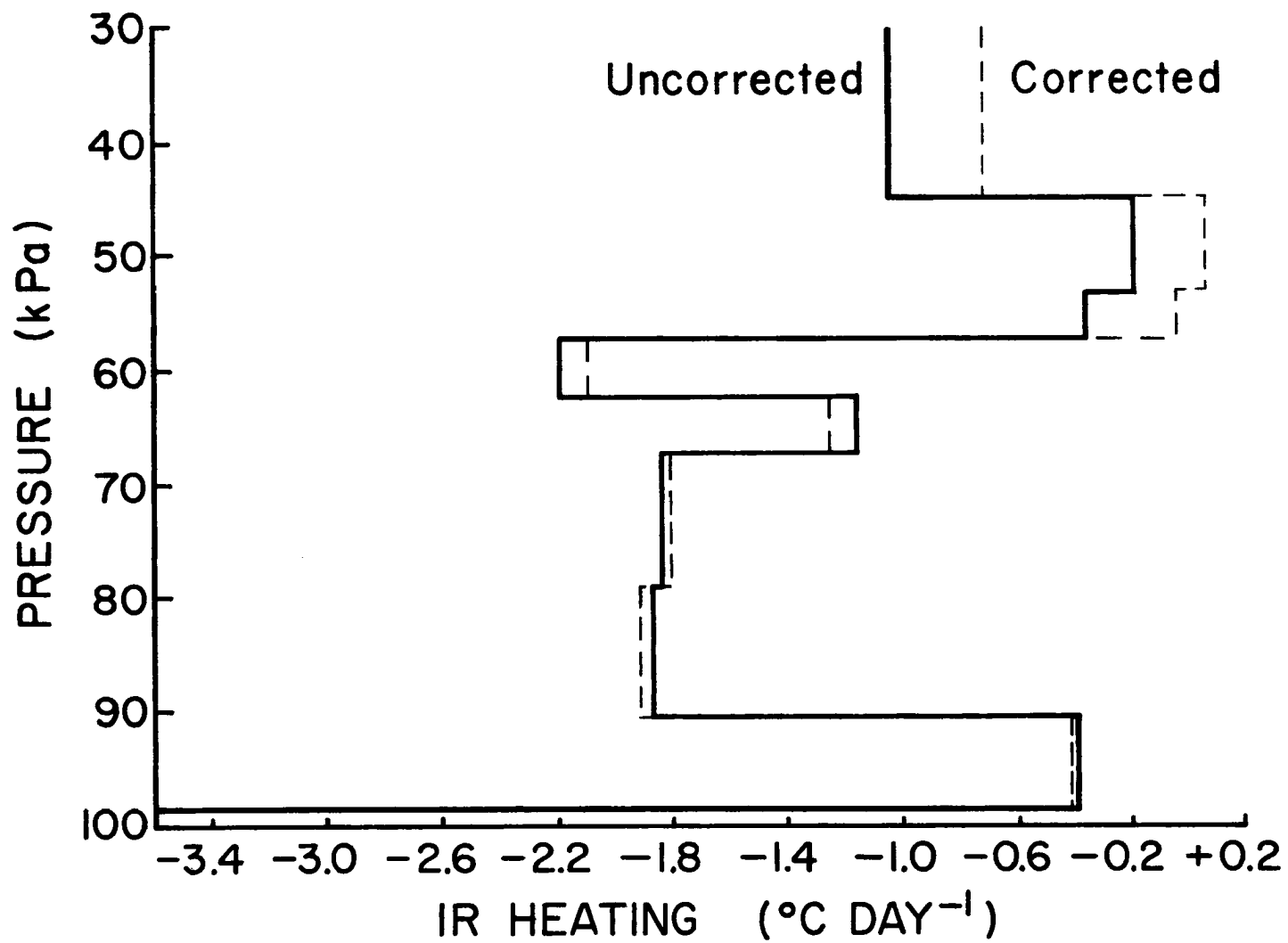


Figure A-8. Infrared heating rates calculated from corrected and uncorrected pyrgeometer measurements.

between the uncorrected downward irradiance averaged over the first two minutes of each leg and the last two minutes is compared to a similar difference calculated from the corrected data. If the actual downward irradiance is assumed to be constant, then the difference between the first two minutes and last two minutes should be small. The results shown in Table 1 indicate that, in general, this difference is approximately 4 Wm^{-2} smaller for the corrected data than the same difference calculated with the uncorrected data. The differences in some cases, however, are large for both the corrected and uncorrected data. These large differences may be due to horizontal variations in the actual downward irradiance. The largest differences also occur at higher levels where the k values determined previously were significantly larger than the 1.35 value used to make these corrections.

A further comparison of corrected and uncorrected data is shown in Figs. A-9a and b. These measurements were made from the Sabliner on July 30, 1974. The flight pattern flown during the 15 minutes of data shown consisted of a descent from 87.0 kPa to 94.2 kPa from 13:45:00 to 13:48:30. The 94.2 kPa pressure level was maintained until 13:50:30 at which time the aircraft ascended to 92.5 kPa and maintained this level until 13:56:00. The data shown from 13:57:30 to 13:60:00 were recorded at a pressure level of 91.0 kPa. The transient response of the instrument is quite evident in the uncorrected data, with variations as large as $\pm 4 \text{ Wm}^{-2}$ occurring during a particular leg. In most cases, the corrections reduce these variations to less than $\pm 1.5 \text{ Wm}^{-2}$.

Table A-1a. Average of first two minutes
minus average of last two
minutes of each leg for upward
facing pyrgeometer.

RUN I			RUN II		
P(kPa)	Uncorrected	Corrected	P(kPa)	Uncorrected	Corrected
28.82	-26.1	-21.1	53.20	-15.2	-12.3
45.27	30.1	21.3	57.60	5.3	2.8
53.27	8.7	4.8	62.50	1.4	0
57.8	4.3	.1	67.50	5.8	1.9
62.6	9.8	3.9	72.97	2.4	0
67.9	7.5	2.4	78.62	4.0	-2.3
78.95	3.8	0	84.70	2.5	-1.3
90.80	6.4	1.3	92.70	1.5	.9
98.80	4.7	2.1	101.10	6.8	3.3
100.03	.4	1.9			

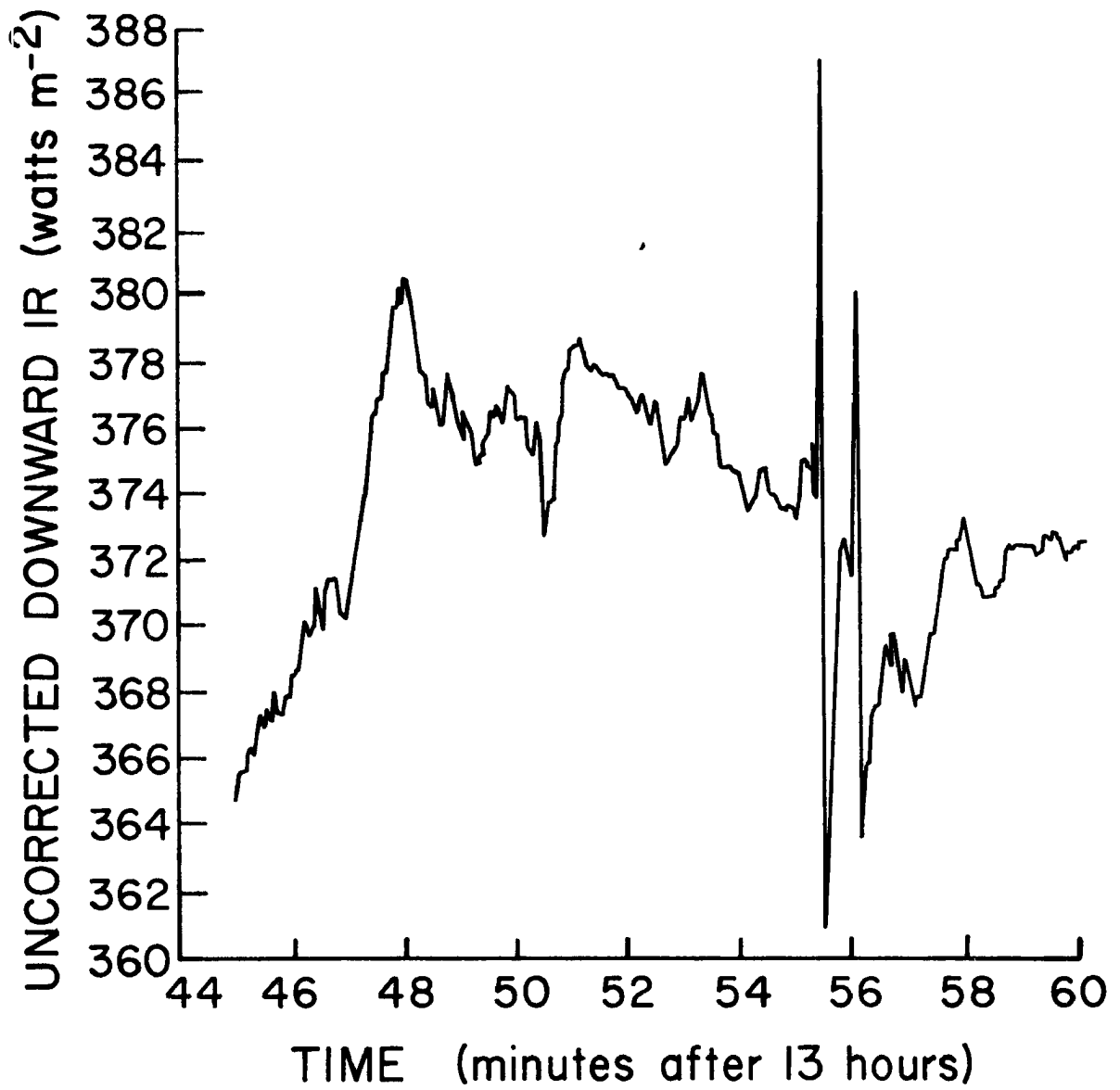


Figure A-9a. Uncorrected pyrgeometer measurements for July 30, 1974, Sabreliner flight.

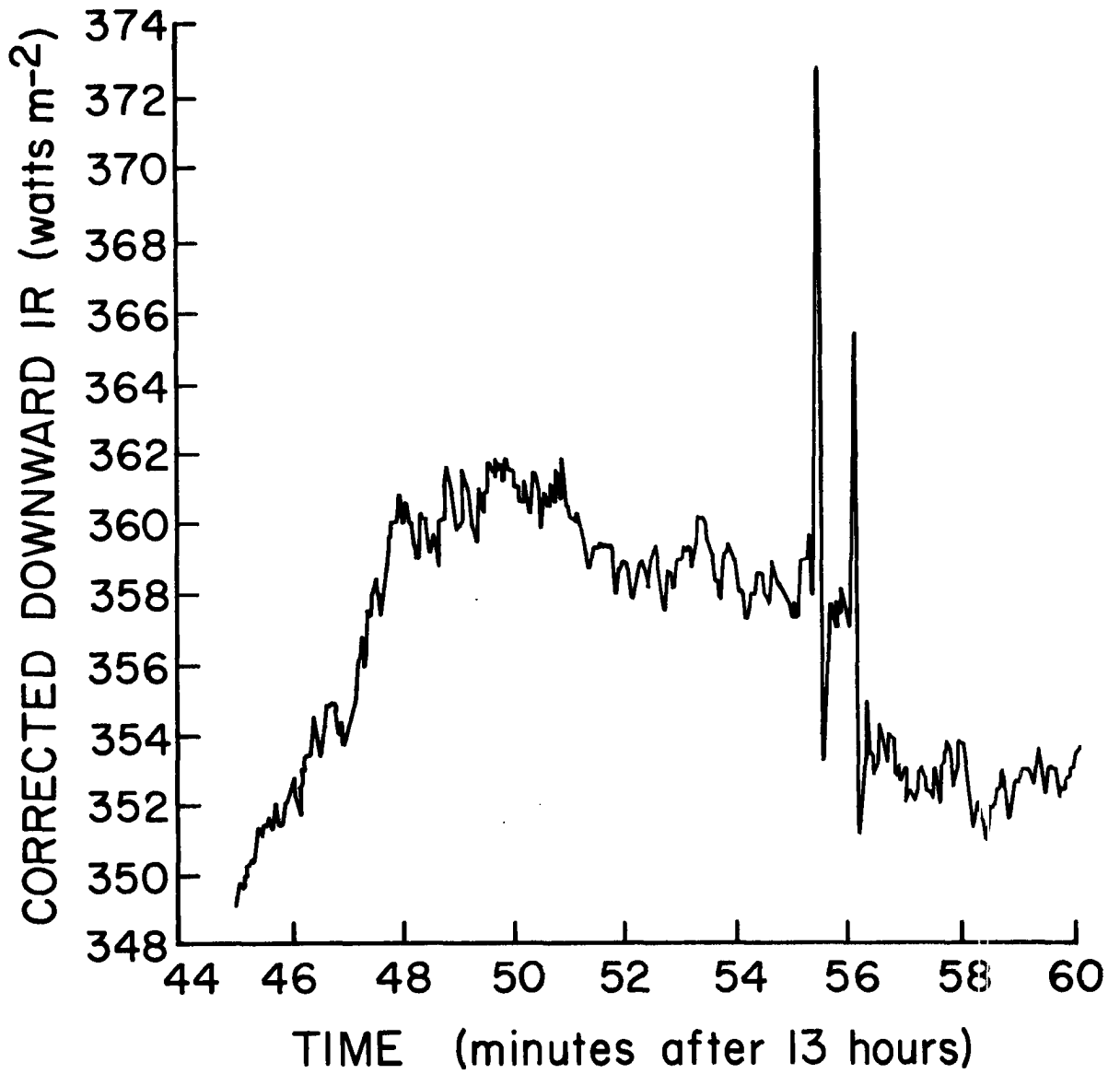


Figure A-9b. Corrected pyrgeometer measurements for July 30, 1974, Sabreliner flight.

A.V. CONCLUSIONS AND RECOMMENDATIONS

Eppley pyrgeometer measurements made from aircraft may be subject to several sources of error. The principal errors identified in this report are due to (1) uncertainties in battery voltages, (2) non-linearity of circuitry at extreme temperatures and (3) errors due to differential heating of the instrument. Although these errors may be large in the absolute sense (as large as 50 Wm^{-2}), they do not appear to affect the net radiation if the upward and downward facing instruments are at the same equilibrium temperatures.

The errors in the output may be largely eliminated if independent measurements of the dome and sink temperatures are made. These corrections not only reduce the absolute errors significantly but also significantly decrease the transient response of the instrument.

From the results obtained in this report, it appears that measuring dome and sink temperatures and monitoring battery voltages and using this information to decompose the pyrgeometer output and obtain the corrected output may not be the most efficient means of making pyrgeometer measurements from aircraft. It may be more efficient to simply accurately measure the thermopile output and the dome and sink temperatures and to determine the measured irradiance in the reduction of the data. Another alternative would be to sophisticate the internal circuitry of the pyrgeometer to eliminate the errors discussed above.

Regardless of the method used to improve the precision of the Eppley pyrgeometer, instruments designed specifically for aircraft should be equipped with separate external connectors for instrument output (or thermopile output) and thermistor measurements. The mv output is easily contaminated by condensation within the connector providing a conductive path to other pins on the connector.

Additional pyrgeometer data also needs to be analyzed in order that the k value needed to make the dome-sink correction can be determined at various temperatures and air speeds. An analysis of this type may be useful in evaluating the validity of determining the dome temperature from a single point measurement.

REFERENCES

Albrecht, B., M. Poellot, and S. K. Cox, 1974: Pyrgeometer Measurements from Aircraft. Rev. Sci. Instrum., 45, No. 1, pp. 33-38.

APPENDIX B

DC-6 SOLAR HEATING CORRECTION FOR LW+ MEASUREMENTS

TABLE OF CONTENTS

	<u>PAGE</u>
B-I. INTRODUCTION	72
B-II. METHOD OF CORRECTION	72
B-III. RESULTS	80
B-IV. CONCLUSIONS	83

B-I. INTRODUCTION

As mentioned in Appendix A, the airflow over the pyrgeometers tends to minimize the heating of the KRS-5 hemisphere due to the absorption of solar radiation. However, for slower moving aircraft (e.g. the U.S. DC-6) the airflow may not be sufficient to prevent solar heating of the dome. This is evident in the L_{\downarrow} and H_{\downarrow} measurements shown in Fig. B-1. These measurements were made at 1300Z, September 7, 1974, over the GATE array from the DC-6. The pressure level of the aircraft during this time is 1002 mb and the free air temperature is approximately 25.5°C. The L_{\downarrow} data shown in Fig. B-1 appears to be strongly correlated to the downward irradiance. Physically, however, one would expect very little or slightly negative correlation between these two parameters at this level in the atmosphere.

The positive correlation between the downward longwave and downward shortwave is consistent with the variations in temperature differences between the dome and sink. This is shown in Fig. B-2 where 30 second averages of a correction factor based on measured dome and sink temperature differences are shown to be correlated with the downward irradiance values averaged for the same time interval. It should be noted that the intercept of the temperature correction shown in Fig. B-2 has not been calibrated absolutely. The relative variations will be consistent, however, since air temperature is approximately constant during this period.

B-II. METHOD OF CORRECTION

The data presented in Fig. B-1 and Fig. B-2 indicate that a correction on L_{\downarrow} may be expressed directly in terms of the downward irradiance. This method of correcting the heating of the dome due to solar radiation on the

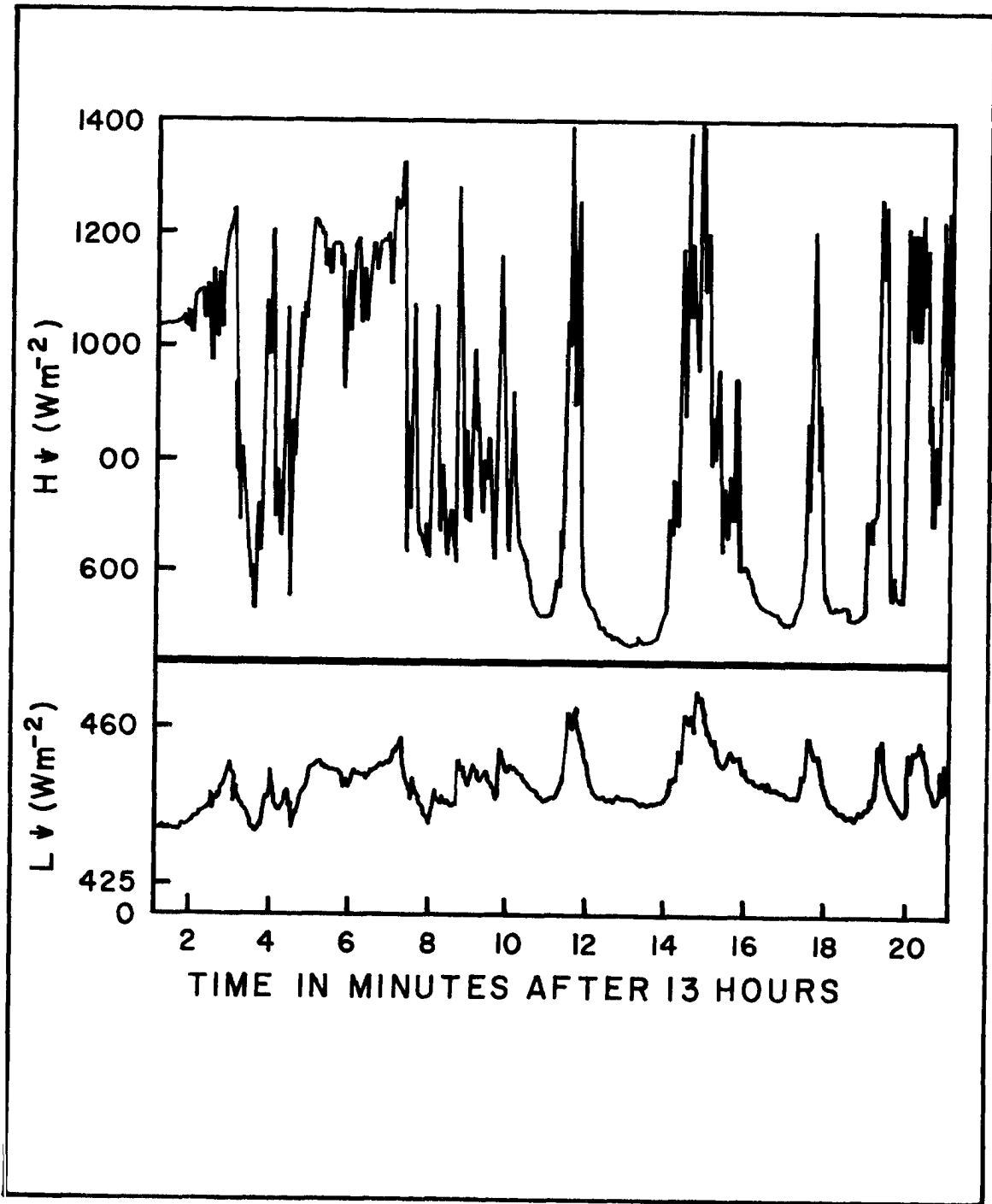


Figure B-1. DC-6 L+ and H+ measurements.
September 7, 1974, 1301-1321 GMT.

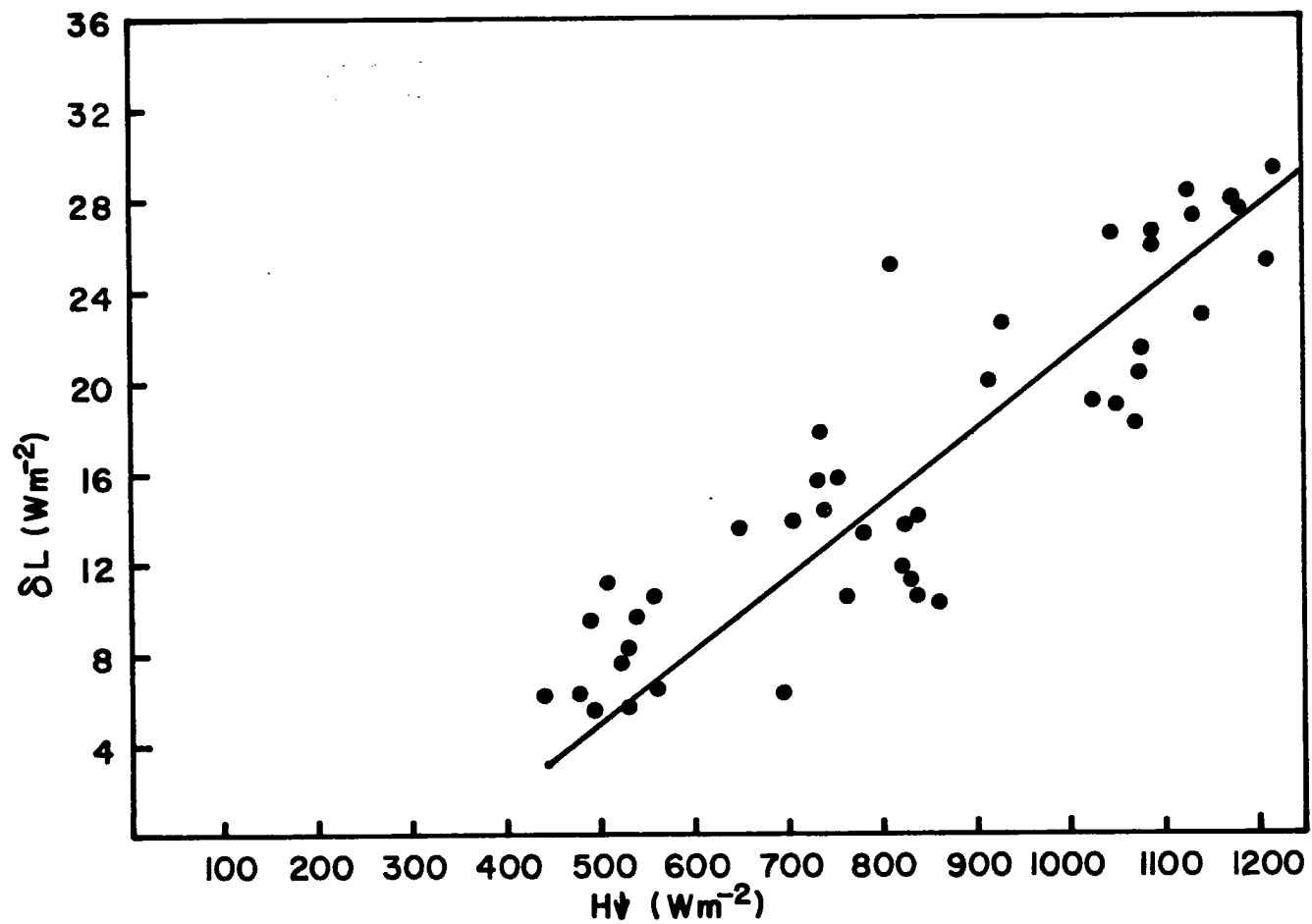


Figure B-2. $L\downarrow$ correction based on difference between dome and sink temperature as a function of $H\downarrow$. All values are 30 second averages.

DC-6 is appealing since 1) the temperature difference between the dome and sink was not determined for the entire GATE, 2) the dome temperature is determined at a single point so that a correction derived from this data may depend on solar and aircraft geometry, and 3) the intercept value of the correction is not known to any certainty on this particular aircraft.

To determine a correction formula based on the incident solar radiation, an equation of the form

$$\delta L = a H_{\downarrow} + b \frac{\partial H_{\downarrow}}{\partial t} \quad (1)$$

where $L_{\downarrow \text{corr}} = L_{\downarrow} + \delta L$, and a and b are constants is assumed. The derivative of the downward shortwave irradiance represents a backward derivative in time and is included in Eq. 1 since intuitively it is logical that the desired correction may depend on the "past" heating history of the dome.

Some care must be used in determining the constants a and b in Eq. 1 since the corrections are on the order of 5% of the absolute value of L_{\downarrow} . Ideally, to determine the constants from data it is desirable to have measurements in a region where the downward irradiance is constant and the downward shortwave varies with time. In the tropical atmosphere such conditions are approximately satisfied near the surface with a scattered cloud field above. This property is illustrated by noting the downward irradiance fields calculated for a typical clear sky tropical atmosphere shown in Fig. B-3. Note that if a black cloud $\epsilon=1.0$ with a cloud base at 950 mb was placed in this atmosphere, the downward irradiance near the surface would only differ slightly from the clear sky value. Note, further that if measurements are made beneath a broken homogeneous cumulus field the downward irradiance would remain fairly constant since the pyrgeometer is

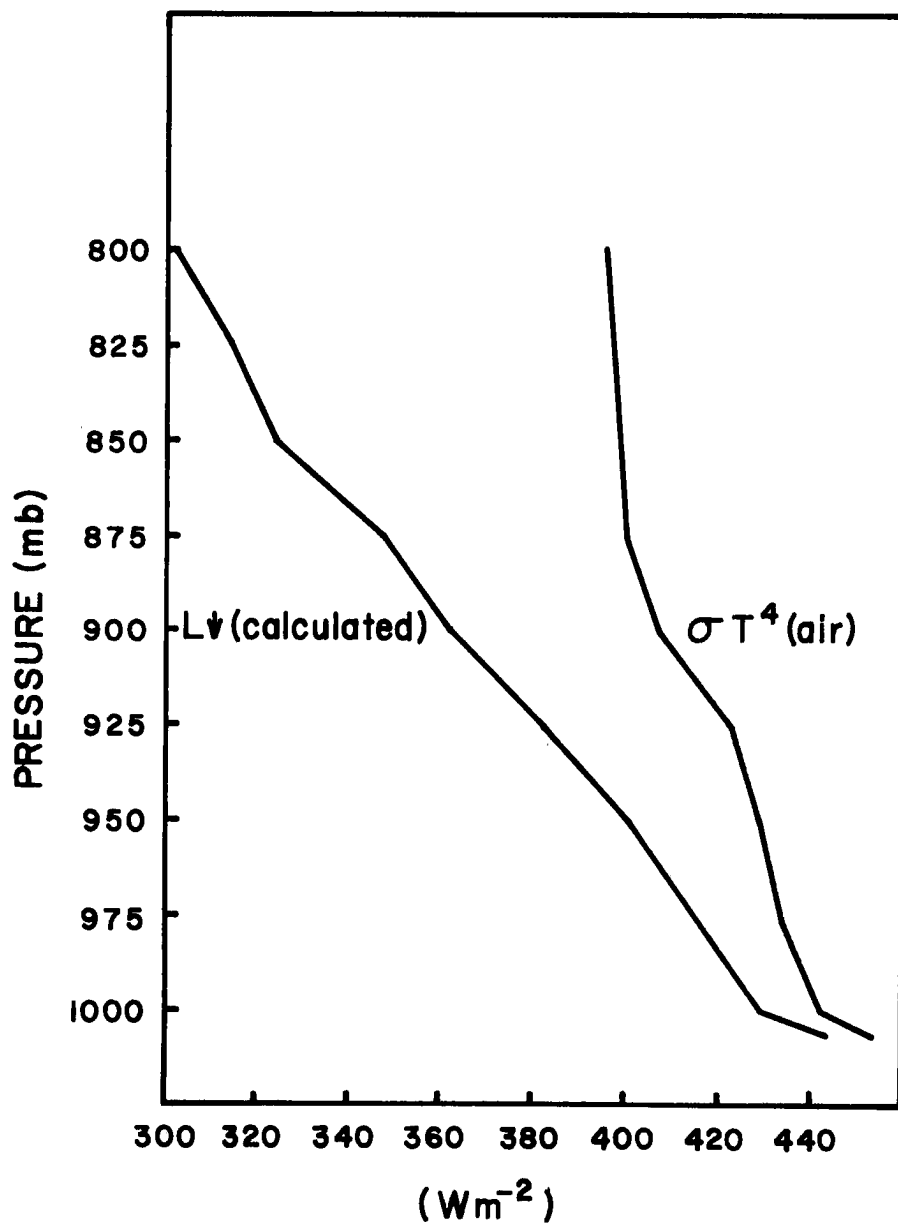


Figure B-3. Calculated downward LW irradiance for a typical tropical atmosphere and $\sigma T^4(\text{air})$ for this same atmosphere.

a hemispheric instrument. The downward shortwave irradiance in this case, however, would vary significantly due to the contribution of the direct radiation.

The assumption that the downward longwave is constant over some interval is used on the data shown in Fig. B-1 to deduce appropriate values of a and b in Eq. 1. The coefficient a is determined by plotting the measured $L\downarrow$ as a function of $H\downarrow$ at points where $\left(\frac{\partial H\downarrow}{\partial t}\right)_i^*$ is approximately zero ($\leq 15 \text{ Wm}^{-2} \text{ sec}^{-1}$). Data collected from 1301 to 1308 and meeting these criteria are plotted in Fig. B-4. Although there is some scatter of these points, the fit is not unreasonable considering that the actual $L\downarrow$ may vary by a few Wm^{-2} . The coefficient, a, may also be determined by noting that if Eq. 1 is averaged over some interval $t_1 < t < t_2$ it becomes

$$\delta L = aH\downarrow + \frac{b[H(t_2) - H(t_1)]}{t_2 - t_1} \quad (2)$$

note that if the interval is sufficiently large, the second term may be neglected reducing Eq. 2 to

$$\delta \bar{L} = a\bar{H}\downarrow.$$

Fifteen second averages of $L\downarrow$ and $H\downarrow$ are plotted in Fig. B-5 for the 1301-1308. The data have been subjectively stratified into three time periods to account for the apparent large-scale variations in the actual $L\downarrow$. The slopes of the lines are identical with the slope shown in Fig. B-4 and nearly identical to the slope shown in Fig. B-2 which was based on dome and sink temperature differences.

The coefficient b is determined by plotting $L\downarrow_{\text{meas}} - a\bar{H}\downarrow + \eta$ as a function of $\left(\frac{\partial H\downarrow}{\partial t}\right)_i$ where η is a parameter which attempts to account for

*: $\left(\frac{\partial H\downarrow}{\partial t}\right)_i$ is defined here as $(H_i - H_{i-2}) / 2$ where H_i is the value of irradiance at the i^{th} second.

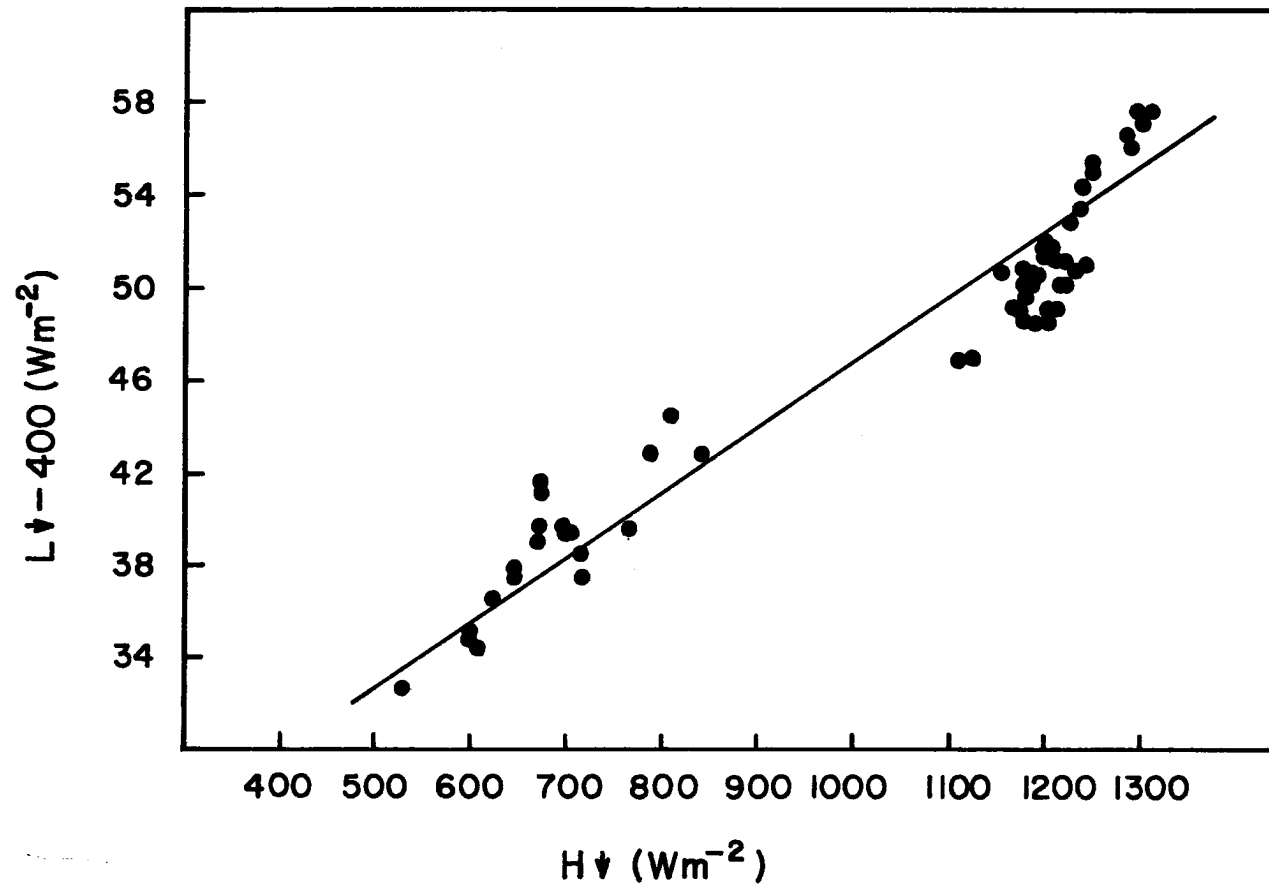


Figure B-4. $L\downarrow$ as a function of $H\downarrow$ at points where $\frac{\partial L\downarrow}{\partial t} \leq 15 \text{ Wm}^{-2} \text{ sec}^{-1}$.

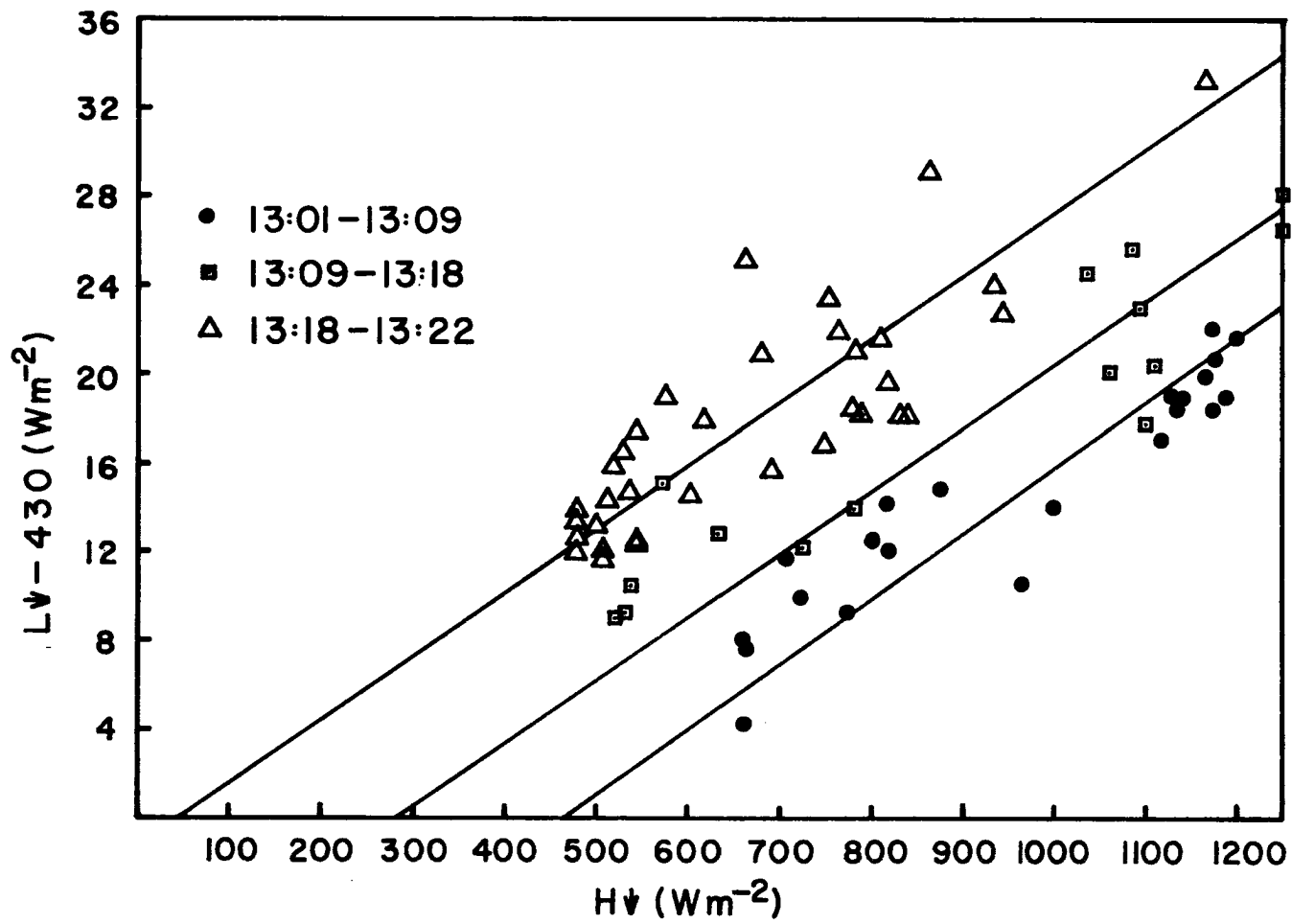


Figure B-5. 15 second averages of $L\downarrow$ and $H\downarrow$ stratified into three separate time intervals.

the actual variations in the downward longwave. The factor η was determined by assuming that the deviations of the points from the line shown in Fig. B-4 may be attributed to real variations in L_{\downarrow} . These deviations implied by this subjective analysis are plotted as a function of time and subsequently extrapolated to all data points.

B-III. RESULTS

A plot of $L_{\downarrow \text{meas}} - aH_{\downarrow} + \eta$ as a function of $\left(\frac{\partial H_{\downarrow}}{\partial t}\right)_-$ was made for the 1301 to 1308 time period and is shown in Fig. B-6. Although there is considerable scatter, the negative correlation is clearly discernable. Physically, this is consistent with the idea that $L_{\downarrow \text{meas}}$ will slightly lag the solar irradiance.

The results presented above give an expression for the correction as

$$L_{\downarrow \text{corr}} = L_{\downarrow \text{meas}} - .0311 H_{\downarrow} + .0666 \left(\frac{\partial H_{\downarrow}}{\partial t}\right)_- . \quad (3)$$

Eq. 3, written in finite difference form is

$$L_{\downarrow \text{corr}} = L_{\downarrow \text{meas}} + .022 H_i - .0333 H_{i-2} \quad (4)$$

The corrected value of L_{\downarrow} calculated from Eq. 4 was calculated for 1308 to 1318 time period of the September 7, 1974, DC-6 flight. The shortwave down, uncorrected and corrected longwave down for this period are shown in Fig. B-7. The average value for this period is decreased from 449 Wm^{-2} for the uncorrected data to 427 Wm^{-2} for the corrected data. The standard deviation for this same period decreased from 7.0 Wm^{-2} to 3.9 Wm^{-2} . It is important to note that although the standard deviation is still relatively high, the variations in the corrected data are of a much higher frequency than those in the uncorrected data. Consequently, these variations would be more easily filtered from the data than the variations which appear in the uncorrected data.

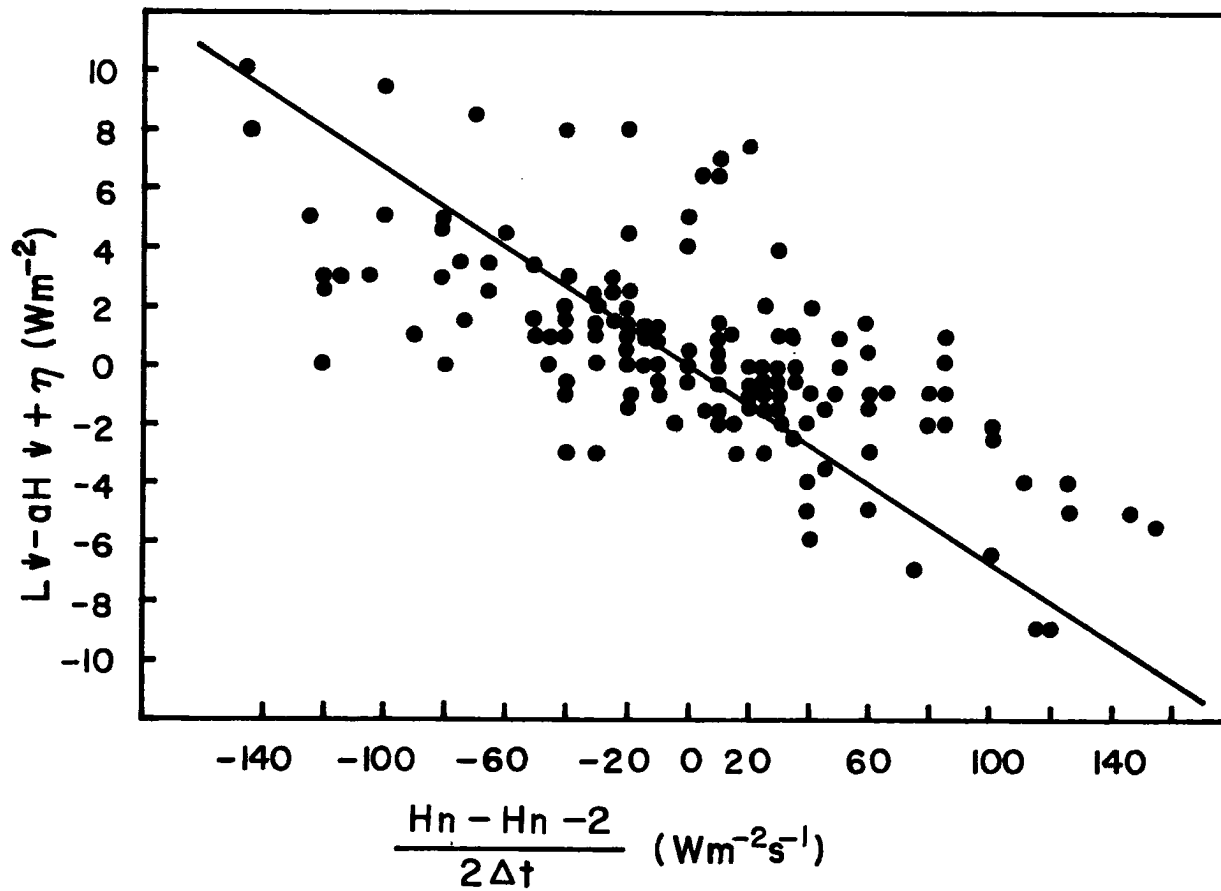


Figure B-6. A plot of $L_{\downarrow \text{meas}} - aH_{\downarrow} + \eta$ as a function of $\left(\frac{\partial H}{\partial t}\right)_{-}$ for the 1301-1308 time period.

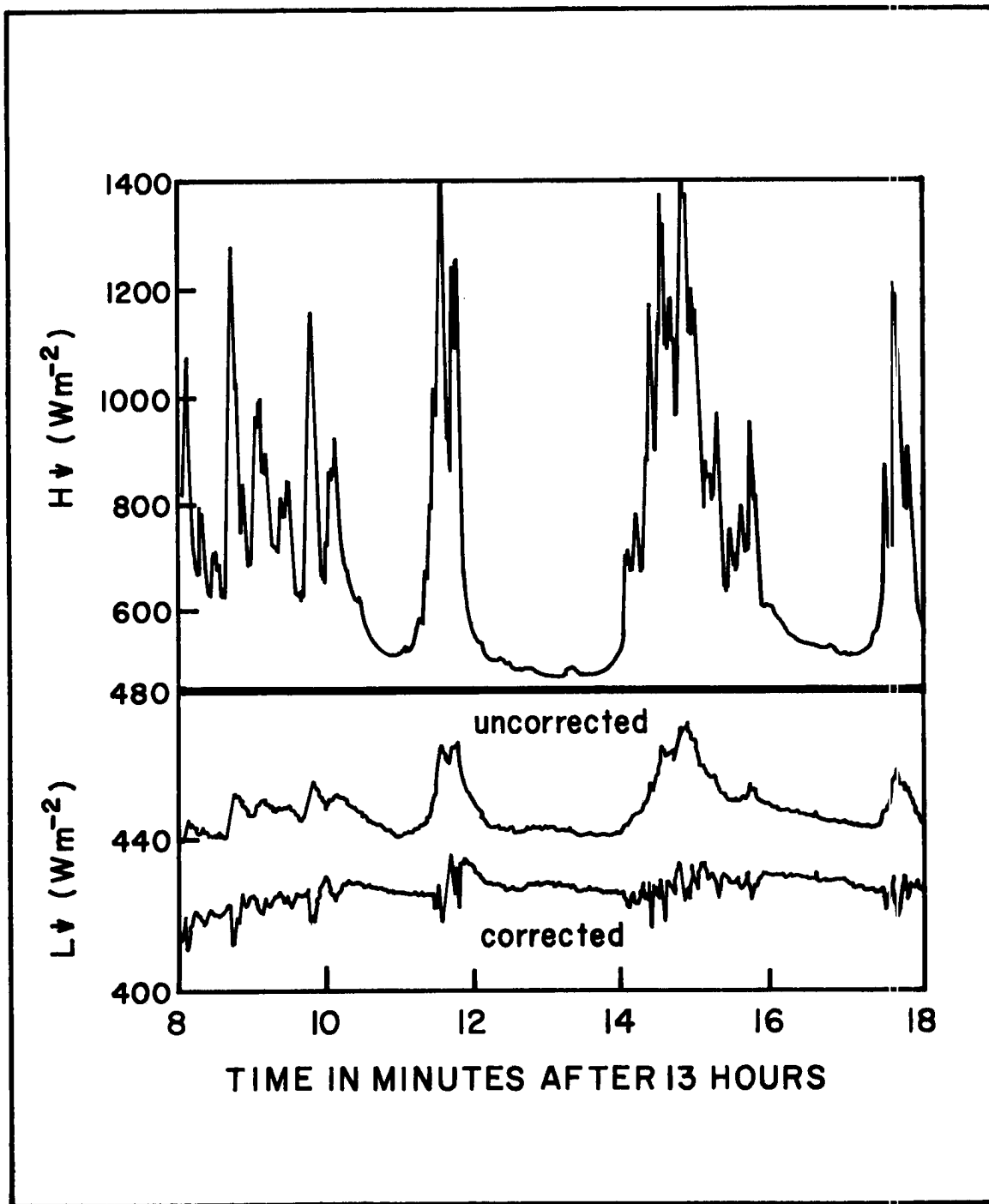


Figure B-7. A comparison of corrected and uncorrected L↓ for the September 7, 1974, DC-6 flight.

B-IV. CONCLUSIONS

An empirical expression may be derived to correct pyrgeometer measurements for the effect of solar heating of the KRS-5 hemisphere. In this study, simultaneous observations of the solar irradiance and the time variation of the solar irradiance are used to correct the downward infrared observations. The empirical correction decreased the average value of L_{\downarrow} for a representative local noon case by 22 Wm^{-2} and decreased the standard deviation of L_{\downarrow} for the same period from 7.0 to 3.9 Wm^{-2} .

APPENDIX C

DATA FLAGGING CRITERIA

On the Sabreliner, C-130 and DC-6 reduced radiation data, a series of data quality indicators, hereafter referred to as flags, have been assigned to each data point. These flags are integer numerals between 1 and 9. The meaning of each integer value is given in Table C1a. Table C1b summarizes the meaning of the integer flags used for one minute average GATE Aircraft Data.

Table C2 lists the criteria used to assign a numerical flag value of 4 to data from the DC-6 and the C-130. All "in pod" data points as well as nighttime conditions will be flagged questionable by using these criteria. Table C3 gives the corresponding flagging criteria used for the Sabreliner. Table C4 gives the methodology used to determine the maximum allowable values of H.

Table C5 gives the criteria used to check for discontinuities in the data. This criteria is dependent upon the time constant of the instrument and is most useful for discriminating short bursts of radio frequency interference.

- 5 Manually flagged questionable (not flagged by machine)
- 6 Before takeoff or after landing
- 9 Missing

Table Clb. Validity Flags for 1-minute Average GATE Aircraft Data

<u>Flag #</u>	<u>Means that data is:</u>
1	The average of 60 good 1 sec ⁻¹ data points
2	" " " 50-59 good 1 sec ⁻¹ data points
3	" " " 40-49 " " " " "
4	" " " 30-39 " " " " "
5	" " " 20-29 " " " " "
6	" " " 10-19 " " " " "
7	" " " 1-9 " " " " "
9	All 60 data points questionable data missing.

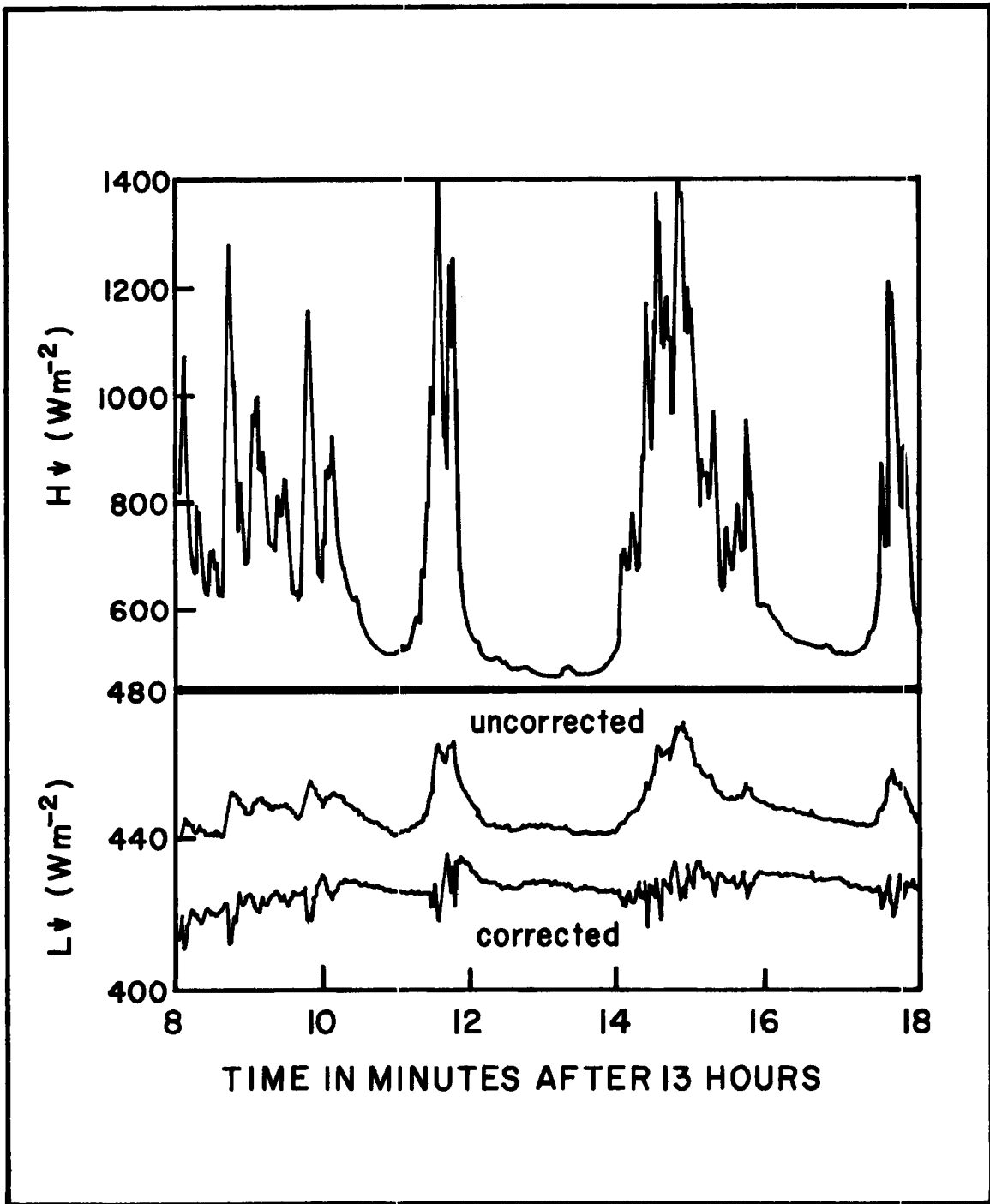


Figure B-7. A comparison of corrected and uncorrected L_{\downarrow} for the September 7, 1974, DC-6 flight.

B-IV. CONCLUSIONS

An empirical expression may be derived to correct pyrgeometer measurements for the effect of solar heating of the KRS-5 hemisphere. In this study, simultaneous observations of the solar irradiance and the time variation of the solar irradiance are used to correct the downward infrared observations. The empirical correction decreased the average value of L_{\downarrow} for a representative local noon case by 22 Wm^{-2} and decreased the standard deviation of L_{\downarrow} for the same period from 7.0 to 3.9 Wm^{-2} .

APPENDIX C

DATA FLAGGING CRITERIA

On the Sabreliner, C-130 and DC-6 reduced radiation data, a series of data quality indicators, hereafter referred to as flags, have been assigned to each data point. These flags are integer numerals between 1 and 9. The meaning of each integer value is given in Table C1a. Table C1b summarizes the meaning of the integer flags used for one minute average GATE Aircraft Data.

Table C2 lists the criteria used to assign a numerical flag value of 4 to data from the DC-6 and the C-130. All "in pod" data points as well as nighttime conditions will be flagged questionable by using these criteria. Table C3 gives the corresponding flagging criteria used for the Sabreliner. Table C4 gives the methodology used to determine the maximum allowable values of H .

Table C5 gives the criteria used to check for discontinuities in the data. This criteria is dependent upon the time constant of the instrument and is most useful for discriminating short bursts of radio frequency interference.

Table Cla. Validity Flags for 1 sec⁻¹ GATE Aircraft Data

<u>Flag #</u>	<u>Means that data is:</u>
1	O.K.
2	Machine flagged questionable; manual edit indicates data acceptable.
3	Unvalidated
4	Machine flagged questionable
5	Manually flagged questionable (not flagged by machine)
6	Before takeoff or after landing
9	Missing

Table Clb. Validity Flags for 1-minute Average GATE Aircraft Data

<u>Flag #</u>	<u>Means that data is:</u>
1	The average of 60 good 1 sec ⁻¹ data points
2	" " " 50-59 good 1 sec ⁻¹ data points
3	" " " 40-49 " " " " "
4	" " " 30-39 " " " " "
5	" " " 20-29 " " " " "
6	" " " 10-19 " " " " "
7	" " " 1-9 " " " " "
9	All 60 data points questionable data missing.

TABLE C2.

DATA QUALITY FLAGGING CRITERIA FOR C-130 & DC-6 RADIATION DATA

The criteria used for flagging DC-6 and C-130 radiation data as questionable (FLAG = 2) are summarized below. These criteria should be applied to the data in the same order as they appear below. All other data may be flagged as probably good (FLAG = 1).

	LWD		LWU		SWD		SWU
1	LWU < 100 Wm ⁻²		LWU < 100		LWU < 100		LWU < 100
2	SWD < 10		SWD < 10		SWD < 10		SWD < 10
3	LWD < 100 or LWD > FLBB*+20	C-130	LWU > 510 or LWU < FLBB*-20		SWD > Hmax(t)**		SWU < .03 x SWD or SWU > .8 x SWD
	LWD < 200 or LWD > FLBB*+20	DC-6					
	LWD > FLBB						

* FLBB = 315 + 5.25 T_{FL} where T_{FL} is flight level free air temperature in °C.

** Hmax(t) is given in attached tables as a function of time.

If Hmax(t) = 0, do not apply criteria (1) and (2); apply (3) only. If the criteria are met flag the data as questionable. If the criteria of (3) are not met flag as not looked at.

TABLE C3.

DATA QUALITY FLAGGING CRITERIA FOR SABRELINER RADIATION DATA

The criteria used for flagging Sabreliner radiation data as questionable (FLAG = 2) are summarized below. These criteria should be applied to the data in the same order as they appear below. All other data may be flagged as probably good (FLAG = 1). (Pending manual edit.)

STEP NO.	LWD	LWU	SWD	SWU
1	$LWD < 50 \text{ Wm}^{-2}$	$LWU < FLBB^* - 10$	$SWD < 0$	$SWU < .03 \times SWD$
2	$LWD > FLBB^* + 10$	$LWU > 510$	$SWD > H_{max}(t)^{**}$	$SWU > .8 \times SWD$

* $FLBB(\text{Wm}^{-2}) = \sigma T_{FL}^4$ where T_{FL} is flight level free air temperature in degrees absolute and
 $\sigma = 5.70 \times 10^{-8} \text{ Wm}^{-2} \cdot \text{K}^4$ Sabreliner only.

** $H_{max}(t)$ is given in attached tables as a function of time.

$$H_{\max}(t) = -A \cos \left[\frac{2\pi}{24} \left(t - \frac{\text{longitude}}{15^\circ} \right) \right] + 200 \quad (1)$$

where t is GMT and given in hours, longitude is given in degrees west and A values are given below.

Aircraft	A (Wm^{-2})
DC-6	1130
C-130	1280
S/L	1280

Note that if $H_{\max}(t)$ given by Eq. (1) is less than 0, that $H_{\max}(t) = 0$.

Consequently, $H_{\max}(t) = 0$ if $6.5 > \left(t - \frac{\text{longitude}}{15^\circ} \right) > 17.5$.

Table C4 Analytical approximations to the $H_{\max}(t)$ values given in Table 1.

AIRCRAFT	$\frac{\Delta LWD}{\Delta t}$ ($Wm^{-2}sec^{-1}$)	$\frac{\Delta LWU}{\Delta t}$ ($Wm^{-2}sec^{-1}$)	$\frac{\Delta SWD}{\Delta t}$ ($Wm^{-2}sec^{-1}$)	$\frac{\Delta SWU}{\Delta t}$ ($Wm^{-2}sec^{-1}$)
Sabreliner	60	60	.250 $H_{max}^*(t)$.200 $H_{max}(t)$
U.S. C-130	60	60	.250 $H_{max}(t)$.200 $H_{max}(t)$
U.S. DC-6	35	30	.250 $H_{max}(t)$.200 $H_{max}(t)$

* $H_{max}(t)$ is given in table C4 for each aircraft.

Table C5 Maximum Possible Rate of Change of GATE Aircraft Radiation Parameters.

APPENDIX D
GATE DC-6 "QUICK-LOOK" COMMENTS
COMMENTS

DATE	COMMENTS
6/21/74 172	No radiation data.
6/22/74 173	No radiation data.
6/24/74 175	No radiation data.
6/26/74 177	First DC-6 flight with radiation data; radiation parameters extremely noisy, values seem quite unrealistic, input was improperly grounded. Cox 23-24 not operating. Data was not properly recorded or tape. Only available data is from visible display and recorded in notebook.
6/28/74 179	First DC-6 flight with radiation data; radiation parameters extremely noisy, values seem quite unrealistic, input was improperly grounded. Cox 23-24 not operating. Data quality fair. Grounding problems produced serious glitches. Some data useable.
6/30/74 181	" " "
7/2/74 183	Radiation parameters still quite noisy although some data might be retrieved by careful hand inspection.
7/3/74 184	H \downarrow noisy and of an unrealistic magnitude L \downarrow , L \uparrow and H \uparrow appear to be O.K.
7/5/74 186	(Tower fly-by) Radiometers on but retracted in pod, no noise.
7/11/74 192	A few noise spikes were noted, L \downarrow shows some positive correlation with H \downarrow
7/12/74 193	Little if any noise noted, L \downarrow > L \uparrow in some cases, L \downarrow \sim 30 Wm $^{-2}$ > L \uparrow when instruments are retracted in the pods, other parameters are O.K.
7/28/74 209	Only a few noise spikes were noted, L \downarrow appears to be somewhat large, L \downarrow shows a positive correlation with H \downarrow
7/29/74 210	No noise noted; L \downarrow shows correlation with H \downarrow
7/31/74 212	No noise noted; L \downarrow > L \uparrow when instruments are retracted into pod

DATE	COMMENTS
8/1/74 213	No noise noted; some data taken at 740 mb, which may be of interest for calibration purposes; L ₊ may be unrealistically large
8/3/74 215	No noise noted; L ₊ may be unrealistically large, L ₊ correlated with H ₊
8/5/74 217	No noise noted; some missing data, zero offsets appear to be slightly negative on this flight
8/6/74 218	No noise noted; zero offset < 0 on H ₊ , L ₊ may be unrealistically large; Cox 23 and 24 operative on this and remainder of flights
8/10/74 222	Some radio noise noted early in flight; some missing data, H ₊ offset appears to be O.K. L ₊ may be unrealistically large, L ₊ correlated with H ₊
8/11/74 223	No noise noted, L ₊ may be unrealistically large, L ₊ is correlated with H ₊
8/13/74 225	" " "
8/14/74 226	Some radio noise at beginning of flight, L ₊ may be unrealistically large, L ₊ is correlated with H ₊
8/16/74 228	Some missing data; L ₊ may be unrealistically large, L ₊ shows some correlation with H ₊
8/17/74 229	Some noise near end of flight; L ₊ > L ₊ when instruments are retracted
8/30/74 242	Some noise noted, L ₊ is correlated with H ₊
8/31/74 243	LW ₊ > LW ₊ on some of the flight legs; some noise noted during the end of the flight.
9/2/74 245	No noise noted, L ₊ may be correlated to H ₊
9/3/74 246	Some radio noise, L ₊ may be correlated with H ₊ Data all looks good.

DATE	COMMENTS
9/4/74 247	No radiation data, Tower fly-by
9/6/74 249	Some missing data, some radio noise
9/9/74 252	Some missing data, some radio noise, $L_{\uparrow} > L_{\downarrow}$
9/15/74 258	L_{\uparrow} and L_{\downarrow} have approximately the right magnitude during the first part of the flight
9/17/74 260	Some missing data
9/18/74 261	Some radio noise noted
9/20/74 266	Computer down, no data

APPENDIX E

GATE SABRELINER "QUICK-LOOK" COMMENTS-12 December 1975

<u>DAY</u>	<u>COMMENTS</u>
July 23 1974	Data good, no noise noted. All parameters reasonable
July 25 206	" " " "
July 26 207	Corrected downward shortwave † not valid 1137-1158 Other parameters OK
July 27 208	Mission aborted because of mechanical problems, data OK before this time
July 29	Take off - 1038, L†m valid, First day for dome-sink T on top pyrgeometer, L‡ - 1038-1215 zeroed, Other parameters OK
July 30 211	Data good
July 31 212	All parameters missing until 0922, remainder of data good
August 1 213	Data good
August 2 214	Data good
August 3 215	L‡ inoperative often 16:1200 to end of flight, other parameters OK
August 5 217	L‡ small, other parameters OK L‡ inoperative 1238-end of flight
August 8 220	L‡ inoperative during the entire flight, other parameters OK
August 9 221	L‡ appears to be too small, possibly due to battery problem - is negative at some points. Other parameters OK, BTM pyrgeometer sink and dome T
August 10	L‡ inoperative during entire flight, due to battery problem other parameters OK
August 11 223	Data good
August 12 224-1	L‡ inoperative T off to 1116, remainder of L‡ appears to be OK but should be examined carefully
224-2	L† inoperative take off 1538 L‡ inoperative 1506 to end of flight, other parameters OK

<u>DAY</u>	<u>COMMENTS</u>	
August 14 226	L+ not good from take off to 1002 - battery problem L+ invalid until 10:1200 often this time needs to be examined closely, this time appears to be too small (possibly moisture in connector) but may be OK	
August 15 227	L+ bad for entire flight, H+ and H+ OK	
August 16 228	Data good	
August 17 229	Data good	
August 20 232	Data good	
August 22 234	Data good	
August 23 235	No radiation data	
August 24 237	No radiation data	
August 25 237	No temperature correction made on this data, L+ data should be examined closely although it appears to be OK Offset cal. made at end of flight	
August 29 241	L+ inoperative after 1318 Other parameters OK	
August 30 242	No L+ or L+ on this flight, H+ and H+ OK	
August 31 243	Data good	
September 1 244	Data good	
September 4 247	Data good	
September 5 248	Data good	
September 6 249	SW data OK, No LW data	Squall?
September 7 250	No radiation data	

<u>DAY</u>		<u>COMMENTS</u>
September 8 251	Data good No PRT-6	
September 9 252	Data good	
September 11 254	Data good	
September 12 255	Data good	
September 14 257	Data good	
September 16 258	Data good	Squall Line?
September 18 260	Data good, few LW+ values seem too small	
September 19 261	Data good	

APPENDIX F

GATE C-130 "Quick Look" Comments

DATE

6/21/74 172	Bottom pod closed during the entire flight. Values show offsets with thumbwheel switch.
6/23/74 174	Tower fly-bys, no radiation data
6/24/74 175	Data shows offset with the thumbwheel switch. Some of the data may be recovered by a manual edit. Data recorded on magnetic tape for this flight show an offset due to a ground loop when the display unit was monitoring a specific channel.
6/26/74 177	Data shows offset with tee thumbwheel switch. Data quality good, glitches caused by thumbwheel display on DVM. Short switch on channel 6 infrequent lock up.
6/28/74 179	A considerable number of "in pod" and zero values. Late T/O resulted in little useful radiation data.
6/30/74 181	SW+ and LW+ show considerable noise, numerous zero values. Data quality excellent, but HF communication causes jumps of ~.04 in channels 1 and 3.
7/15/74 196	Good data, instruments "in pod" during the last part of the flight.
7/16/74 197	LW+ appears to be inoperative during a small portion of the flight, remainder of data good.
7/27/74 208	No radiation data.
7/28/74 209	No radiation data.
7/29/74 210	No noise noted, data appears to be excellent.
8/1/74 213	Data O.K.
8/2/74 214	Some radiation data was recorded during the first part of the flight, remainder missing.
8/4/74 216	Data appears to be good.

DATE	COMMENTS
8/5/74 217	Many zero calibration values recorded during first and last part of the tape, H+ has considerable noise.
8/7/74 219	No radiation data.
8/10/74 222	Excellent data; no noise. Cal. 3-4 problems in switch and drift.
8/11/74 223	Excellent data early in the flight, noise increases during end of the flight.
8/13/74 225	Data O.K., no noise. All instruments working properly.
8/14/74 226	Data noisy during the first part of the flight. Middle portion of the flight is better in quality but still a large number of zero values. H+ not functioning.
8/17/74 229	Good data during first half of the flight. A large number of zero values during the last half of the flight. No data from top instruments past 100400 due to pod malfunction.
8/30/74 242	Data good, except for H+ which is noisy.
8/31/74 243	Some noise on L+ and H+. L+ zero $\sim +8 \text{ Wm}^{-2}$ Some H+ values very unrealistic. Some missing data near the end of the flight - due to inability to get top pod open.
9/2/74 245	Some noise during early part of flight. No noise during most of the remainder of the flight.
9/3/74 246	Some noise noted.
9/4/74 247	Much noise and many in pod values.
9/5/74 248	Some missing data, many zero calibration values.
9/6/74 249	Some missing data, remainder of other data appears to be good.

DATE	COMMENTS
9/8/74 251	A large number of zero calibration values were noted on this flight. Calibration switch was accidentally hit by A.M.S. - time unknown.
9/9/74 252	L \downarrow and H \downarrow were noted to be noisy.
9/11/74 254	Some radio noise noted, some missing data.
9/12/74 255	Some noise noted, mostly on L \downarrow
9/14/74 257	Downward parameters occasionally noisy.
9/15/74 258	Much of the L \downarrow and H \downarrow values noisy.
9/17/74 260	Some radio noise noted.
9/18/74 261	Considerable radio noise noted on L \downarrow and H \downarrow
9/20/74 263	Many zero values during the first part of the flight.

APPENDIX G

The data parameters on the NOAA/DC-6 are on magnetic tape in the following order and format:

Time in GMT	V Wind Component
Latitude	Static Pressure
Longitude	Radar Altitude
Heading	Temperature
Attach Angle	Dew Point Temperature
N-S Ground Speed	Apparent Surface Temperature
E-W Ground Speed	Liquid Water Content
True Airspeed	Longwave Outgoing Radiation
Pitch Angle	Shortwave Outgoing Radiation
Roll Angle	Longwave Incoming Radiation
U Wind Component	Shortwave Incoming Radiation
	Sideslip Angle
	Quality Flags

(I1, I4, I10, I5, 12 (F6.0, F7.3, F8.3, F5.1, F6.2, F6.1, F5.1, F5.1, F5.1, F5.1, F5.1, F6.1, F5.0, F5.1, F5.1, F4.1, F6.1, F6.1, F6.1, F6.1, F6.2, 23I1))

The data parameters on the NOAA/C-130 are on the tape in the following order and format:

Time in GMT	Aircraft Vertical Velocity
Latitude	Static Pressure
Longitude	Radar Altitude
Heading	Temperature
Sideslip Angle	Dew Point Temperature
Attack Angle	Apparent Surface Temperature
N-S Ground Speed	CO ₂ Temperature
E-W Ground Speed	Longwave Outgoing Radiation
True Airspeed	Shortwave Outgoing Radiation
Roll Angle	Longwave Incoming Radiation
Pitch Angle	Shortwave Incoming Radiation
U Wind Component	Liquid Water Content
V Wind Component	Total Water Content
	Quality Flags

(I1, I4, I10, I, 10 (F6.0, F7.3, F8.3, F5.1, F6.2, F6.2, F6.1, F6.1, F5.1,
F5.1, F5.1, F5.1, F5.1, F5.1, F6.1, F7.1, F5.1, F5.1, F5.1, F6.2, F7.1, F7.1,
F7.1, F7.1, F4.1, F5.2, 26I1))

BIBLIOGRAPHIC DATA SHEET	1. Report No. CSU-ATSP-244	2.	3. Recipient's Accession No.
4. Title and Subtitle Radiation Data Reduction Procedures for Sabreliner, C-130, and DC-6 Aircraft During the GARP Atlantic Tropical Experiment		5. Report Date February 1976	6.
7. Author(s) Dr. Stephen K. Cox and Bruce A. Albrecht		8. Performing Organization Rept. No. CSU-ATSP-244	
9. Performing Organization Name and Address Department of Atmospheric Science Colorado State University Fort Collins, Colorado 80523		10. Project/Task/Work Unit No.	11. Contract/Grant No. NSF & NOAA OCD72-01681 A04 and COD 74-21678
12. Sponsoring Organization Name and Address Global Atmospheric Research Program National Science Foundation Washington, D. C. 20550		13. Type of Report & Period Covered	14.
15. Supplementary Notes			
16. Abstracts <p>This paper presents a description of the basic radiation data gathering systems used on three U.S. Aircraft during the GARP Atlantic Tropical Experiment. In addition to an explanation of the hardware used, the data reduction procedures applied to the raw data are given in detail. Significant problems encountered in the data are also discussed; in some instances remedial steps have been incorporated into the data reduction while in others, the potential user is forewarned about the problems.</p>			
17. Key Words and Document Analysis. 17a. Descriptors <p>Aircraft Radiation Measurements GARP Atlantic Tropical Experiment (GATE)</p> 17b. Identifiers/Open-Ended Terms 17c. COSATI Field/Group			
18. Availability Statement		19. Security Class (This Report) UNCLASSIFIED	21. No. of Pages 100
		20. Security Class (This Page) UNCLASSIFIED	22. Price